Hindawi
Shock and Vibration
Volume 2018, Article ID 8562079, 21 pages
https://doi.org/10.1155/2018/8562079

Research Article

A Series Solution for the Vibration of Mindlin Rectangular Plates with Elastic Point Supports around the Edges

Fuzhen Pang, Haichao Li, Yuan Du, Shuo Li, Hailong Chen, and Ning Liu

College of Shipbuilding Engineering, Harbin Engineering University, Harbin, 150001, China

Correspondence should be addressed to Haichao Li; lihaichao@hrbeu.edu.cn and Yuan Du; duyuan@hrbeu.edu.cn

Received 31 January 2018; Revised 25 April 2018; Accepted 30 April 2018; Published 28 June 2018

Academic Editor: Lorenzo Dozio

A series solution for the transverse vibration of Mindlin rectangular plates with elastic point supports around the edges is studied. The series solution for the problem is obtained using improved Fourier series method, in which the vibration displacements and the cross-sectional rotations of the midplane are represented by a double Fourier cosine series and four supplementary functions. The supplementary functions are expressed as the combination of trigonometric functions and a single cosine series expansion and are introduced to remove the potential discontinuities associated with the original admissible functions along the edges when they are viewed as periodic functions defined over the entire x-y plane. This series solution is approximately accurate in the sense that it explicitly satisfies, to any specified accuracy, both the governing equations and the boundary conditions. The convergence, accuracy, stability, and efficiency of the proposed method have been examined through a series of numerical examples. Some numerical examples about the nondimensional frequency and mode shapes of Mindlin rectangular plates with different point-supported edge conditions are given.

1. Introduction

Rectangular plate is of great importance in various engineering branches, such as aerospace, electronics, and mechanical, nuclear, and marine engineering. A better understanding of its dynamic characteristics is meaningful when dealing with the design of a plate-type structure. In the early stage of research about rectangular plate, the majority of research was about thin plate based on classical Kirchhoff hypothesis. However, for the shortage of consideration about transverse shear deformation and rotary inertia, vibration frequencies of thick plates are overestimated. More and more investigations about Mindlin plates began to attract attention after the Mindlin first-order plate theory was proposed by Mindlin [1]. The vibration characteristics of Mindlin plates have been well investigated by researches with classical and elastic edge support [2–5]. Few literatures focused on the vibration behavior of Mindlin plates with elastic point supports around the edges. However, the boundary conditions of the plates are not always classical and elastic around the edges in practical engineering applications. And the boundary conditions of elastic point supports around the edges do exist. So it is much of great significance to study the vibration behavior of Mindlin plates with elastic point supports around the edges.

In the field of vibration analysis of structures subject to elastic edge/point supports, Takashi and Jin [6] used the collocation method to investigate Mindlin plates with constant thickness and two opposite edges simply supported. Jiarang and Jianqiao [7] established the three-dimensional state equation for the laminated thick orthotropic plate with simply supported edges and obtained the numerical results. Ohya et al. [3] investigated the free vibration characteristics of rectangular Mindlin plates which have simultaneous elastic edge and internal supports via the superposition method. Hosseini-Hashemi et al. [8] proposed an exact closed-form procedure to solve free vibration of moderately thick rectangular plates with two opposite edges simply supported. Dozio et al. [9] developed a Ritz method using a set of trigonometric functions to obtain accurate modal properties of rectangular plates with arbitrary thickness. Maretic [10] analyzed the transverse vibration of a circular plate loaded by uniform pressure along its edge. Based on the shear deformable plate theory, Bahmyari [11] used the Element-Free Galerkin Method to analyze the free vibration of inhomogeneous

moderately thick plates with point supports resting on a two-parameter elastic foundation. The results show that the vibration results obtained are in a very good agreement with the available literatures in spite of using low numbers of nodes. Bashmal et al. [12] investigated the in-plane free vibrations of an elastic and isotropic annular disk with elastic constraints at the inner and outer boundaries. And the inner and outer boundaries are applied either along the entire periphery of the disk or at a point. Esendemir [13] studied polymer-matrix composite beam of arbitrary orientation supported from two ends acted upon with a force at the midpoint by an analytical elastoplastic stress analysis. Foyouzat et al. [14] presented an analytical-numerical approach to determine the dynamic response of thin plates resting on multiple elastic point supports with time-varying stiffness. Gan et al. [15] studied the effect of intermediate elastic support on the vibration of functionally graded Euler-Bernoulli beams excited by a moving point load. Kucuk et al. [16] carried out the analytical elastic-plastic stress analysis on an aluminum metal-matrix composite beam reinforced by unidirectional steel fibers supported at the ends acted upon with a force at the midpoint. Hosseini-Hashemi et al. [17–19] used the generalized differential quadrature method to study the buckling analysis and dynamic transverse vibration characteristics. Setoodeh and Karami [20] employed a three-dimensional elasticity based layerwise finite element method (FEM) to study the static, free vibration, and buckling responses of general laminated thick composite plates. In this paper, the elastic line and point supports are successfully incorporated for thick plates. On the basis of three-dimensional elasticity theory, Xu and Zhou [21] studied the bending of simple-supported rectangular plate on point supports, line supports, and elastic foundation. Wu [22] analyzed the free vibration of arbitrary quadrilateral thick plates with internal columns and elastic edge supports by using the powerful pb-2 Ritz method and Reddy's third-order shear deformation plate theory. Wu and Lu [23] studied the free vibration of rectangular plates with internal columns and elastic edge supports using the powerful pb-2 Ritz method. Other literatures related to this field are shown in [24–28].

From the literatures review, we can know that most researches focused on the classical plates. Only few literatures studied the vibration characteristics of Mindlin plates with point supports around the edges. And these literatures mainly used the collocation method, analytical-numerical method, and so on. To the best of the authors' knowledge, there are no published literatures focused on vibration characteristics of Mindlin plates with point supports around the edges by the method of modified Fourier. Thus, a unified, efficient, and accurate formulation to deal with the free vibration of Mindlin plates subjected to arbitrary point-supported boundary condition is necessary and much of great significance.

In this paper, a modified Fourier solution for the free vibration of Mindlin rectangular plates with elastic point supports around the edges is proposed. The vibration displacements and the cross-sectional rotations of the midplane are represented by a double Fourier cosine series and four supplementary functions. The supplementary functions are in the form of the combination between trigonometric functions and a single cosine series expansion. By importing supplementary functions, the discontinuity of the boundary condition is overcome. The change of the boundary conditions can be easily achieved by only varying the stiffness of the boundary springs around all edges of the plates without involving any change to the solution procedure. The natural frequencies of Mindlin rectangular plates are obtained by using the Rayleigh–Ritz method. Effectiveness and stability of this method will be verified by comparing with the results of FE modeling. Some numerical examples of free vibration for Mindlin rectangular plates with different aspect ratio and thickness are conducted under different point-supported conditions.

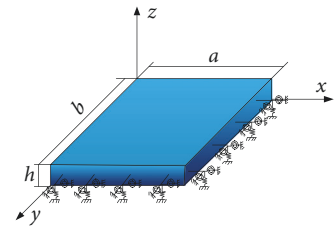

Figure 1: A Mindlin plate with arbitrary elastic point edge supports.

2. Theoretical Formulations

2.1. Point-Supported Edge Conditions. The rectangular Mindlin plate with arbitrary elastic point edge supports is shown in Figure 1. The boundary conditions are presented by three kinds of restraining springs [29–34], namely, translational, rotational, and torsional springs. Springs are evenly arranged on each edge of Mindlin plate. Through changing the stiffness of springs, different boundary conditions can be achieved [35, 36]. The governing differential equations of a Mindlin plate about its free vibration are as follows:

$$kGh\left(\frac{\partial^2 w}{\partial x^2}+\frac{\partial^2 w}{\partial y^2}+\frac{\partial \psi_x}{\partial x}+\frac{\partial \psi_y}{\partial y}\right)-\rho h\frac{\partial^2 w}{\partial t^2}=0 \quad (1)$$

$$D\left(\frac{\partial^2 \psi_x}{\partial x^2}+\frac{1-\mu}{2}\frac{\partial^2 \psi_x}{\partial y^2}+\frac{1+\mu}{2}\frac{\partial^2 \psi_y}{\partial x\partial y}\right)-\kappa Gh\left(\frac{\partial w}{\partial x}+\psi_x\right)-\rho h\frac{\partial^2 \psi_x}{\partial t^2}=0 \quad (2)$$

$$D\left(\frac{\partial^2 \psi_y}{\partial y^2}+\frac{1-\mu}{2}\frac{\partial^2 \psi_y}{\partial x^2}+\frac{1+\mu}{2}\frac{\partial^2 \psi_x}{\partial x\partial y}\right)-\kappa Gh\left(\frac{\partial w}{\partial y}+\psi_y\right)-\rho h\frac{\partial^2 \psi_y}{\partial t^2}=0 \quad (3)$$

In the formulas above, transverse displacement is presented by w, ψ_x is the slope along x direction, and ψ_y is the slope along y direction. ρ means the mass density, μ is Poisson's ratio, κ is the shear correction factor, and the thickness of the plate is h. $G = E/(2(1+\mu))$ is the shear

modulus, μ is Poisson's ratio, and $D = Eh^3/(12(1-\mu^2))$ is the flexural rigidity.

Besides, the bending moment is expressed by (4) and (5), twisting moment is calculated by (6), and the transverse shearing forces in plates are expressed by (7) and (8).

$$M_{xx} = D\left(\frac{\partial \psi_x}{\partial x} + \mu\frac{\partial \psi_y}{\partial y}\right) \tag{4}$$

$$M_{yy} = D\left(\frac{\partial \psi_y}{\partial y} + \mu\frac{\partial \psi_x}{\partial x}\right) \tag{5}$$

$$M_{xy} = \frac{D(1-\mu)}{2}\left(\frac{\partial \psi_x}{\partial y} + \frac{\partial \psi_y}{\partial x}\right) \tag{6}$$

$$Q_x = \kappa G h\left(\psi_x + \frac{\partial w}{\partial x}\right) \tag{7}$$

$$Q_y = \kappa G h\left(\psi_y + \frac{\partial w}{\partial y}\right) \tag{8}$$

There are three kinds of forces along every edge, namely, the bending moment, the twisting moment, and the shearing forces. Rotational, torsional, and translational springs along every edge are the counterparts to these three forces in this paper. The boundary conditions for an elastically restrained rectangular plate are as follows.

At $x = 0$,

$$k_{x0}(y)\, w = -Q_x \tag{9}$$

$$K_{x0}(y)\, \psi_x = -M_{xx} \tag{10}$$

$$K_{yx0}(y)\, \psi_y = -M_{xy} \tag{11}$$

$k_{x0}(y)$, $K_{x0}(y)$, and $K_{yx0}(y)$ represent the stiffness of the translation spring, rotational spring, and torsional spring, respectively, on the boundary edge $x = 0$; the corresponding expression results in

$$k_{x0}(y) = \sum_{i=1}^{N} k_{x0}^i \delta\left(y - y_{x0}^i\right) \tag{12}$$

$$K_{x0}(y) = \sum_{i=1}^{N} K_{x0}^i \delta\left(y - y_{x0}^i\right) \tag{13}$$

$$K_{yx0}(y) = \sum_{i=1}^{N} K_{yx0}^i \delta\left(y - y_{x0}^i\right) \tag{14}$$

where N is the elastic point supports numbers on edge $x = 0$, $\delta(x)$ is the Dirac delta function, and k_{x0}^i, K_{x0}^i, and K_{yx0}^i are, respectively, the stiffness of the translational, rotational, and torsional springs at the i^{th} support located at y_{x0}^i. Similarly, the remaining boundary conditions on the other three edges can be expressed as follows.

At $x = a$,

$$k_{xa}(y)\, w = Q_x \tag{15}$$

$$K_{xa}(y)\, \psi_x = M_{xx} \tag{16}$$

$$K_{yxa}(y)\, \psi_y = M_{xy} \tag{17}$$

$$k_{xa}(y) = \sum_{i=1}^{N} k_{xa}^i \delta\left(y - y_{xa}^i\right) \tag{18}$$

$$K_{xa}(y) = \sum_{i=1}^{N} K_{xa}^i \delta\left(y - y_{xa}^i\right) \tag{19}$$

$$K_{yxa}(y) = \sum_{i=1}^{N} K_{yxa}^i \delta\left(y - y_{xa}^i\right) \tag{20}$$

At $y = 0$,

$$k_{y0}(x)\, w = -Q_y \tag{21}$$

$$K_{y0}(x)\, \psi_y = -M_{yy} \tag{22}$$

$$K_{xy0}(x)\, \psi_x = -M_{xy} \tag{23}$$

$$k_{y0}(x) = \sum_{i=1}^{N} k_{y0}^i \delta\left(x - x_{y0}^i\right) \tag{24}$$

$$K_{y0}(x) = \sum_{i=1}^{N} K_{y0}^i \delta\left(y - y_{y0}^i\right) \tag{25}$$

$$K_{xy0}(x) = \sum_{i=1}^{N} K_{xy0}^i \delta\left(x - x_{y0}^i\right) \tag{26}$$

At $y = b$,

$$k_{yb}(x)\, w = Q_y \tag{27}$$

$$K_{yb}(x)\, \psi_y = M_{yy} \tag{28}$$

$$K_{xyb}(x)\, \psi_x = M_{xy} \tag{29}$$

$$k_{yb}(x) = \sum_{i=1}^{N} k_{yb}^i \delta\left(x - x_{yb}^i\right) \tag{30}$$

$$K_{yb}(x) = \sum_{i=1}^{N} K_{yb}^i \delta\left(x - x_{yb}^i\right) \tag{31}$$

$$K_{yx0}(x) = \sum_{i=1}^{N} K_{yx0}^i \delta\left(y - y_{yb}^i\right) \tag{32}$$

Equations (9)–(32) represent a set of general boundary conditions by setting the spring stiffness to appropriate values. Based on (4)–(8), the boundary condition can be finally written as follows.

At $x = 0$,

$$\sum_{i=1}^{N} k_{x0}^i \delta\left(y - y_{x0}^i\right) w = -\kappa G h\left(\psi_x + \frac{\partial w}{\partial x}\right) \tag{33}$$

$$\sum_{i=1}^{N} K_{x0}^{i}\delta\left(y-y_{x0}^{i}\right)\psi_x = -D\left(\frac{\partial\psi_x}{\partial x}+\mu\frac{\partial\psi_y}{\partial y}\right) \tag{34}$$

$$\sum_{i=1}^{N} K_{yx0}^{i}\delta\left(y-y_{x0}^{i}\right)\psi_y = -\frac{D(1-\mu)}{2}\left(\frac{\partial\psi_x}{\partial y}+\frac{\partial\psi_y}{\partial x}\right) \tag{35}$$

At $x = a$,

$$\sum_{i=1}^{N} k_{xa}^{i}\delta\left(y-y_{xa}^{i}\right)w = \kappa Gh\left(\psi_x+\frac{\partial w}{\partial x}\right) \tag{36}$$

$$\sum_{i=1}^{N} K_{xa}^{i}\delta\left(y-y_{xa}^{i}\right)\psi_x = D\left(\frac{\partial\psi_x}{\partial x}+\mu\frac{\partial\psi_y}{\partial y}\right) \tag{37}$$

$$\sum_{i=1}^{N} K_{yxa}^{i}\delta\left(y-y_{xa}^{i}\right)\psi_y = \frac{D(1-\mu)}{2}\left(\frac{\partial\psi_x}{\partial y}+\frac{\partial\psi_y}{\partial x}\right) \tag{38}$$

At $y = 0$,

$$\sum_{i=1}^{N} k_{y0}^{i}\delta\left(x-x_{y0}^{i}\right)w = -\kappa Gh\left(\psi_y+\frac{\partial w}{\partial y}\right) \tag{39}$$

$$\sum_{i=1}^{N} K_{y0}^{i}\delta\left(y-y_{y0}^{i}\right)\psi_y = -D\left(\frac{\partial\psi_y}{\partial y}+\mu\frac{\partial\psi_x}{\partial x}\right) \tag{40}$$

$$\sum_{i=1}^{N} K_{xy0}^{i}\delta\left(x-x_{y0}^{i}\right)\psi_x = -\frac{D(1-\mu)}{2}\left(\frac{\partial\psi_x}{\partial y}+\frac{\partial\psi_y}{\partial x}\right) \tag{41}$$

At $y = b$,

$$\sum_{i=1}^{N} k_{yb}^{i}\delta\left(x-x_{yb}^{i}\right)w = \kappa Gh\left(\psi_y+\frac{\partial w}{\partial y}\right) \tag{42}$$

$$\sum_{i=1}^{N} K_{yb}^{i}\delta\left(x-x_{yb}^{i}\right)\psi_y = D\left(\frac{\partial\psi_y}{\partial y}+\mu\frac{\partial\psi_x}{\partial x}\right) \tag{43}$$

$$\sum_{i=1}^{N} K_{yx0}^{i}\delta\left(y-y_{yb}^{i}\right)\psi_x = \frac{D(1-\mu)}{2}\left(\frac{\partial\psi_x}{\partial y}+\frac{\partial\psi_y}{\partial x}\right) \tag{44}$$

According to the Mindlin plate theory, the transverse displacement of the plate middle surface and the rotations of the cross section, respectively, along the x direction and the y direction are utilized. Based on the traditional solution method, the admissible functions usually express a Fourier series expansion, because the Fourier functions constitute a complete set and exhibit an excellent numerical stability in the previous study [37–43]. We found the conventional Fourier series expression to have some defects which contain the convergence problem along the boundary edges except for a few simple boundary conditions, and the derivatives of a Fourier series cannot be obtained simply through term-by-term differentiation.

In this study, in order to overcome the shortcoming with the conventional Fourier series expression, the admissible functions will be expressed as a more wholesome form of Fourier series expansion:

$$\begin{aligned} w(x,y) = {} & \sum_{m=0}^{\infty}\sum_{n=0}^{\infty} A_{mn}\cos\lambda_{am}x\cos\lambda_{bn}y \\ & + \sum_{l=1}^{2}\zeta_b^l(y)\sum_{m=0}^{\infty} a_m^l\cos\lambda_{am}x \\ & + \sum_{l=1}^{2}\zeta_a^l(x)\sum_{n=0}^{\infty} b_n^l\cos\lambda_{bn}y \end{aligned} \tag{45}$$

$$\begin{aligned} \psi_x(x,y) = {} & \sum_{m=0}^{\infty}\sum_{n=0}^{\infty} B_{mn}\cos\lambda_{am}x\cos\lambda_{bn}y \\ & + \sum_{l=1}^{2}\zeta_b^l(y)\sum_{m=0}^{\infty} c_m^l\cos\lambda_{am}x \\ & + \sum_{l=1}^{2}\zeta_a^l(x)\sum_{n=0}^{\infty} d_n^l\cos\lambda_{bn}y \end{aligned} \tag{46}$$

$$\begin{aligned} \psi_y(x,y) = {} & \sum_{m=0}^{\infty}\sum_{n=0}^{\infty} C_{mn}\cos\lambda_{am}x\cos\lambda_{bn}y \\ & + \sum_{l=1}^{2}\zeta_b^l(y)\sum_{m=0}^{\infty} e_m^l\cos\lambda_{am}x \\ & + \sum_{l=1}^{2}\zeta_a^l(x)\sum_{n=0}^{\infty} f_n^l\cos\lambda_{bn}y \end{aligned} \tag{47}$$

where A_{mn}, a_m^l, b_n^l, B_{mn}, c_m^l, d_n^l, C_{mn}, e_m^l, and f_n^l represent the unknown coefficients, $\lambda_{am} = m\pi/a$, $\lambda_{bn} = n\pi/b$. The specific expressions of the auxiliary functions ζ_a^l and ζ_b^l are defined as

$$\zeta_a^1(x) = \frac{a}{2\pi}\sin\left(\frac{\pi x}{2a}\right)+\frac{a}{2\pi}\sin\left(\frac{3\pi x}{2a}\right) \tag{48}$$

$$\zeta_a^2(x) = -\frac{a}{2\pi}\cos\left(\frac{\pi x}{2a}\right)+\frac{a}{2\pi}\cos\left(\frac{3\pi x}{2a}\right) \tag{49}$$

$$\zeta_b^1(y) = \frac{b}{2\pi}\sin\left(\frac{\pi y}{2b}\right)+\frac{b}{2\pi}\sin\left(\frac{3\pi y}{2b}\right) \tag{50}$$

$$\zeta_b^2(y) = -\frac{b}{2\pi}\cos\left(\frac{\pi y}{2b}\right)+\frac{b}{2\pi}\cos\left(\frac{3\pi y}{2b}\right) \tag{51}$$

As shown in (45)–(47), the supplementary functions ζ_a^1, ζ_a^2, ζ_b^1, and ζ_b^2 are used for the x and y direction displacement expressions. It is easy to find that

$$\zeta_a^1(0) = \zeta_a^1(a) = \zeta_a^{1'}(a) = 0, \quad \zeta_a^{1'}(0) = 1 \tag{52}$$

$$\zeta_a^2(0) = \zeta_a^2(a) = \zeta_a^{2'}(0) = 0, \quad \zeta_a^{2'}(a) = 1 \tag{53}$$

Similar conditions are present in the supplementary function in y-direction, namely, $\zeta_b^1(y)$ and $\zeta_b^2(y)$. Whereas these conditions are not necessary, the existence of these conditions is purely for the sake of simplifying follow-up mathematical expressions and derivation process.

Examining the admissible functions in (45)–(47), one will notice that, besides the standard 2D Fourier series defined

over the domain $\mathfrak{R}^2 : ((0,a)\otimes(0,b))$, four additional 1D Fourier expansions are also included in the admissible functions expressions. In light of (52), it is not difficult to see that the fourth term (or the third single Fourier series) on the right side of (45) is equal to the normal derivative of the displacement function $w(x,y)$ at edge $x=0$. Thus, this term will actually inherit any potential discontinuity associated with the normal derivative at the boundary $x=0$. Similarly, the other three terms are used to take care of the possible discontinuities at the remaining edges. Thus, the 2D Fourier expansion will now represent a periodic Π^2 (residual displacement) function defined over the entire x-y plane. The convergence characteristic for the Fourier series representation of such a function has been well established in mathematics. Namely, the Fourier series will converge with a speed of $(m\pi)^3$ at least.

By substituting (45)–(47) into boundary condition (33) and expanding all the y-related terms, except for those containing $k_{x0}(y)$, into Fourier cosine series, one will have

$$\begin{aligned}
&\sum_{i=1}^{N}\overline{k}_{x0}^{i}\delta\left(y-y_{x0}^{i}\right)\left(\sum_{m=0}^{\infty}\sum_{n=0}^{\infty}A_{mn}\cos\lambda_{bn}y\right.\\
&\quad\left.+\zeta_b^1(y)\sum_{m=0}^{\infty}a_m^1+\zeta_b^2(y)\sum_{m=0}^{\infty}a_m^2\right)\\
&\quad=-\left(\sum_{m=0}^{\infty}\sum_{n=0}^{\infty}B_{mn}\cos\lambda_{bn}y+\sum_{n=0}^{\infty}\beta_{1n}\cos\lambda_{bn}y\sum_{m=0}^{\infty}c_m^1\right.\\
&\quad\left.+\sum_{n=0}^{\infty}\beta_{1n}\cos\lambda_{bn}y\sum_{m=0}^{\infty}c_m^2+\sum_{n=0}^{\infty}b_n^1\cos\lambda_{bn}y\right)
\end{aligned}\tag{54}$$

The expressions for Fourier cosine expansion coefficient of related functions can be found in Appendix A. To establish the relationship between the Fourier coefficients in (54), the terms on the left side shall also be expressed in the form of cosine series, resulting in

$$\begin{aligned}
&\sum_{m=0}^{\infty}\sum_{t=0}^{\infty}A_{mt}\sum_{i=1}^{N}\overline{k}_{x0}^{i}\cos\lambda_{bt}y_{x0}^{i}\cos\lambda_{bn}y_{x0}^{i}\\
&\quad+\sum_{m=0}^{\infty}a_m^1\sum_{i=1}^{N}\overline{k}_{x0}^{i}\zeta_b^1\left(y_{x0}^{i}\right)\cos\lambda_{bn}y_{x0}^{i}\\
&\quad+\sum_{m=0}^{\infty}a_m^2\sum_{i=1}^{N}\overline{k}_{x0}^{i}\zeta_b^2\left(y_{x0}^{i}\right)\cos\lambda_{bn}y_{x0}^{i}=-\overline{\delta}_{bn}\sum_{m=0}^{\infty}B_{mn}\\
&\quad-\overline{\delta}_{bn}\beta_{1n}\sum_{m=0}^{\infty}c_m^1-\overline{\delta}_{bn}\beta_{2n}\sum_{m=0}^{\infty}c_m^2-\overline{\delta}_{bn}b_n^1
\end{aligned}\tag{55}$$

$$\overline{\delta}_{bn}=\frac{b}{2}\left(1+\delta_{0n}\right)\tag{56}$$

$$\overline{\delta}_{am}=\frac{a}{2}\left(1+\delta_{0m}\right)\tag{57}$$

where δ_{0n} and δ_{0m} are Kronecker delta. Using similar procedures, the other seven boundary condition equations can be obtained. Thus, a total of twelve constraint equations can be derived as follows.

At $x=0$,

$$\begin{aligned}
&\sum_{m=0}^{\infty}\sum_{t=0}^{\infty}A_{mt}\sum_{i=1}^{N}\overline{k}_{x0}^{i}\cos\lambda_{bt}y_{x0}^{i}\cos\lambda_{bn}y_{x0}^{i}\\
&\quad+\sum_{m=0}^{\infty}a_m^1\sum_{i=1}^{N}\overline{k}_{x0}^{i}\zeta_b^1\left(y_{x0}^{i}\right)\cos\lambda_{bn}y_{x0}^{i}\\
&\quad+\sum_{m=0}^{\infty}a_m^2\sum_{i=1}^{N}\overline{k}_{x0}^{i}\zeta_b^2\left(y_{x0}^{i}\right)\cos\lambda_{bn}y_{x0}^{i}=-\overline{\delta}_{bn}\sum_{m=0}^{\infty}B_{mn}\\
&\quad-\overline{\delta}_{bn}\beta_{1n}\sum_{m=0}^{\infty}c_m^1-\overline{\delta}_{bn}\beta_{2n}\sum_{m=0}^{\infty}c_m^2-\overline{\delta}_{bn}b_n^1
\end{aligned}\tag{58}$$

$$\begin{aligned}
&\sum_{m=0}^{\infty}\sum_{t=0}^{\infty}B_{mt}\sum_{i=1}^{N}\overline{K}_{x0}^{i}\cos\lambda_{bt}y_{x0}^{i}\cos\lambda_{bn}y_{x0}^{i}\\
&\quad+\sum_{m=0}^{\infty}c_m^1\sum_{i=1}^{N}\overline{K}_{x0}^{i}\zeta_b^1\left(y_{x0}^{i}\right)\cos\lambda_{bn}y_{x0}^{i}\\
&\quad+\sum_{m=0}^{\infty}c_m^2\sum_{i=1}^{N}\overline{K}_{x0}^{i}\zeta_b^2\left(y_{x0}^{i}\right)\cos\lambda_{bn}y_{x0}^{i}\\
&\quad=-\left(\overline{\delta}_{bn}d_n^1-\mu\overline{\delta}_{bn}\sum_{m=0}^{\infty}\sum_{q=0}^{\infty}C_{mt}\lambda_{bq}\kappa_{bn}^{q}\right)\\
&\quad+\overline{\delta}_{bn}\mu\eta_{1n}\sum_{m=0}^{\infty}e_m^1+\overline{\delta}_{bn}\mu\eta_{2n}\sum_{m=0}^{\infty}e_m^2
\end{aligned}\tag{59}$$

$$\begin{aligned}
&\sum_{m=0}^{\infty}\sum_{t=0}^{\infty}C_{mt}\sum_{i=1}^{N}\overline{K}_{yx0}^{i}\cos\lambda_{bt}y_{x0}^{i}\cos\lambda_{bn}y_{x0}^{i}\\
&\quad+\sum_{m=0}^{\infty}e_m^1\sum_{i=1}^{N}\overline{K}_{yx0}^{i}\zeta_b^1\left(y_{x0}^{i}\right)\cos\lambda_{bn}y_{x0}^{i}\\
&\quad+\sum_{m=0}^{\infty}e_m^2\sum_{i=1}^{N}\overline{K}_{yx0}^{i}\zeta_b^2\left(y_{x0}^{i}\right)\cos\lambda_{bn}y_{x0}^{i}\\
&\quad=-\left(-\overline{\delta}_{bn}\sum_{m=0}^{\infty}\sum_{q=0}^{\infty}B_{mq}\lambda_{bq}\kappa_{bn}^{q}+\overline{\delta}_{bn}\eta_{1n}\sum_{m=0}^{\infty}c_m^1\right)\\
&\quad-\overline{\delta}_{bn}\eta_{2n}\sum_{m=0}^{\infty}c_m^2+\overline{\delta}_{bn}f_n^1
\end{aligned}\tag{60}$$

At $x=a$,

$$\begin{aligned}
&\sum_{m=0}^{\infty}\sum_{t=0}^{\infty}(-1)^m A_{mt}\sum_{i=1}^{N}\overline{k}_{x0}^{i}\cos\lambda_{bt}y_{x0}^{i}\cos\lambda_{bn}y_{x0}^{i}\\
&\quad+\sum_{m=0}^{\infty}(-1)^m a_m^1\sum_{i=1}^{N}\overline{k}_{x0}^{i}\zeta_b^1\left(y_{x0}^{i}\right)\cos\lambda_{bn}y_{x0}^{i}\\
&\quad+\sum_{m=0}^{\infty}(-1)^m a_m^2\sum_{i=1}^{N}\overline{k}_{x0}^{i}\zeta_b^2\left(y_{x0}^{i}\right)\cos\lambda_{bn}y_{x0}^{i}\\
&\quad=\overline{\delta}_{bn}\sum_{m=0}^{\infty}(-1)^m B_{mn}+\overline{\delta}_{bn}\beta_{1n}\sum_{m=0}^{\infty}(-1)^m c_m^1\\
&\quad+\overline{\delta}_{bn}\beta_{2n}\sum_{m=0}^{\infty}(-1)^m c_m^2+\overline{\delta}_{bn}b_n^1
\end{aligned}\tag{61}$$

$$\sum_{m=0}^{\infty}\sum_{q=0}^{\infty}(-1)^m B_{mq}\sum_{i=1}^{N}\overline{K}_{x0}^{i}\cos\lambda_{bn}y_{x0}^{i}\cos\lambda_{bq}y_{x0}^{i}$$
$$+\sum_{m=0}^{\infty}(-1)^m c_m^1\sum_{i=1}^{N}\overline{K}_{x0}^{i}\zeta_b^1\left(y_{x0}^{i}\right)\cos\lambda_{bn}y_{x0}^{i}$$
$$+\sum_{m=0}^{\infty}(-1)^m c_m^2\sum_{i=1}^{N}\overline{K}_{x0}^{i}\zeta_b^2\left(y_{x0}^{i}\right)\cos\lambda_{bn}y_{x0}^{i}=\overline{\delta}_{bn}d_n^2 \quad (62)$$
$$-\mu\overline{\delta}_{bn}\sum_{m=0}^{\infty}\sum_{q=0}^{\infty}(-1)^m C_{mq}\lambda_{bq}\kappa_{bn}^{q}$$
$$-\overline{\delta}_{bn}\mu\eta_{1n}\sum_{m=0}^{\infty}(-1)^m e_m^1-\overline{\delta}_{bn}\mu\eta_{2n}\sum_{m=0}^{\infty}(-1)^m e_m^2$$

$$\sum_{m=0}^{\infty}\sum_{q=0}^{\infty}(-1)^m C_{mq}\sum_{i=1}^{N}\overline{K}_{yx0}^{i}\cos\lambda_{bq}y_{x0}^{i}\cos\lambda_{bn}y_{x0}^{i}$$
$$+\sum_{m=0}^{\infty}(-1)^m e_m^1\sum_{i=1}^{N}\overline{K}_{yx0}^{i}\zeta_b^1\left(y_{x0}^{i}\right)\cos\lambda_{bn}y_{x0}^{i}$$
$$+\sum_{m=0}^{\infty}(-1)^m e_m^2\sum_{i=1}^{N}\overline{K}_{yx0}^{i}\zeta_b^2\left(y_{x0}^{i}\right)\cos\lambda_{bn}y_{x0}^{i} \quad (63)$$
$$=-\overline{\delta}_{bn}\sum_{m=0}^{\infty}\sum_{q=0}^{\infty}(-1)^m B_{mq}\lambda_{bq}\kappa_{bn}^{q}$$
$$+\overline{\delta}_{bn}\eta_{1n}\sum_{m=0}^{\infty}(-1)^m c_m^1+\overline{\delta}_{bn}\eta_{2n}\sum_{m=0}^{\infty}(-1)^m c_m^2$$
$$+\overline{\delta}_{bn}f_n^2$$

At $y=0$,

$$\sum_{s=0}^{\infty}\sum_{n=0}^{\infty}A_{sn}\sum_{i=1}^{N}\overline{k}_{y0}^{i}\cos\lambda_{as}x_{y0}^{i}\cos\lambda_{am}x_{y0}^{i}+\sum_{n=0}^{\infty}b_n^1\sum_{i=1}^{N}\overline{k}_{y0}^{i}$$
$$\cdot\zeta_a^1\left(x_{y0}^{i}\right)\cos\lambda_{am}x_{y0}^{i}+\sum_{n=0}^{\infty}b_n^2\sum_{i=1}^{N}\overline{k}_{y0}^{i}\zeta_a^2\left(x_{y0}^{i}\right)\cos\lambda_{am} \quad (64)$$
$$\cdot x_{y0}^{i}=-\left(\overline{\delta}_{am}\sum_{n=0}^{\infty}C_{mn}+\overline{\delta}_{am}\alpha_{1m}\sum_{n=0}^{\infty}f_n^1\right.$$
$$\left.+\overline{\delta}_{am}\alpha_{2m}\sum_{n=0}^{\infty}f_n^2+\overline{\delta}_{am}a_m^1\right)$$

$$\sum_{s=0}^{\infty}\sum_{n=0}^{\infty}C_{mn}\sum_{i=1}^{N}\overline{K}_{y0}^{i}\cos\lambda_{as}x_{y0}^{i}\cos\lambda_{am}x_{y0}^{i}+\sum_{n=0}^{\infty}f_n^1$$
$$\cdot\sum_{i=1}^{N}\overline{K}_{y0}^{i}\zeta_a^1\left(x_{y0}^{i}\right)\cos\lambda_{am}x_{y0}^{i}+\sum_{n=0}^{\infty}f_n^2$$
$$\cdot\sum_{i=1}^{N}\overline{K}_{y0}^{i}\zeta_a^2\left(x_{y0}^{i}\right)\cos\lambda_{am}x_{y0}^{i}=-\left(\overline{\delta}_{am}e_m^1\right. \quad (65)$$
$$-\mu\overline{\delta}_{am}\sum_{s=0}^{\infty}\sum_{n=0}^{\infty}B_{mn}\lambda_{as}\tau_{am}^{s}-\mu\overline{\delta}_{am}\gamma_{1m}\sum_{n=0}^{\infty}d_n^1$$
$$\left.-\mu\overline{\delta}_{am}\gamma_{2m}\sum_{n=0}^{\infty}d_n^2\right)$$

$$\sum_{s=0}^{\infty}\sum_{n=0}^{\infty}B_{sn}\sum_{i=1}^{N}\overline{K}_{xy0}^{i}\cos\lambda_{as}x_{y0}^{i}\cos\lambda_{am}x_{y0}^{i}+\sum_{n=0}^{\infty}d_n^1$$
$$\cdot\sum_{i=1}^{N}\overline{K}_{xy0}^{i}\zeta_a^1\left(x_{y0}^{i}\right)\cos\lambda_{am}x_{y0}^{i}+\sum_{n=0}^{\infty}d_n^2\sum_{i=1}^{N}\overline{K}_{xy0}^{i} \quad (66)$$
$$\cdot\zeta_a^2\left(x_{y0}^{i}\right)\cos\lambda_{am}x_{y0}^{i}=-\left(-\overline{\delta}_{am}\sum_{s=0}^{\infty}\sum_{n=0}^{\infty}C_{sn}\lambda_{as}\tau_{am}^{s}\right.$$
$$\left.+\overline{\delta}_{am}\gamma_{1m}\sum_{n=0}^{\infty}f_n^1+\overline{\delta}_{am}\gamma_{2m}\sum_{n=0}^{\infty}f_n^2+\overline{\delta}_{am}c_m^1\right)$$

At $y=b$,

$$\sum_{s=0}^{\infty}\sum_{n=0}^{\infty}(-1)^n A_{sn}\sum_{i=1}^{N}\overline{k}_{y0}^{i}\cos\lambda_{as}x_{y0}^{i}\cos\lambda_{am}x_{y0}^{i}$$
$$+\sum_{n=0}^{\infty}(-1)^n b_n^1\sum_{i=1}^{N}\overline{k}_{y0}^{i}\zeta_a^1\left(x_{y0}^{i}\right)\cos\lambda_{am}x_{y0}^{i}$$
$$+\sum_{n=0}^{\infty}(-1)^n b_n^2\sum_{i=1}^{N}\overline{k}_{y0}^{i}\zeta_a^2\left(x_{y0}^{i}\right)\cos\lambda_{am}x_{y0}^{i} \quad (67)$$
$$=\overline{\delta}_{am}\sum_{n=0}^{\infty}(-1)^n C_{mn}+\overline{\delta}_{am}\alpha_{1m}\sum_{n=0}^{\infty}(-1)^n f_n^1$$
$$+\overline{\delta}_{am}\alpha_{2m}\sum_{n=0}^{\infty}(-1)^n f_n^2+\overline{\delta}_{am}a_m^2$$

$$\sum_{s=0}^{\infty}\sum_{n=0}^{\infty}(-1)^n C_{sn}\sum_{i=1}^{N}\overline{K}_{y0}^{i}\cos\lambda_{as}x_{y0}^{i}\cos\lambda_{am}x_{y0}^{i}$$
$$+\sum_{n=0}^{\infty}(-1)^n f_n^1\sum_{i=1}^{N}\overline{K}_{y0}^{i}\zeta_a^1\left(x_{y0}^{i}\right)\cos\lambda_{am}x_{y0}^{i}$$
$$+\sum_{n=0}^{\infty}(-1)^n f_n^2\sum_{i=1}^{N}\overline{K}_{y0}^{i}\zeta_a^2\left(x_{y0}^{i}\right)\cos\lambda_{am}x_{y0}^{i}=\overline{\delta}_{am}e_m^2 \quad (68)$$
$$-\mu\overline{\delta}_{am}\sum_{s=0}^{\infty}\sum_{n=0}^{\infty}(-1)^n B_{mn}\lambda_{as}\tau_{am}^{s}$$
$$-\mu\overline{\delta}_{am}\gamma_{1m}\sum_{n=0}^{\infty}(-1)^n d_n^1-\mu\overline{\delta}_{am}\gamma_{2m}\sum_{n=0}^{\infty}(-1)^n d_n^2$$

$$\sum_{s=0}^{\infty}\sum_{n=0}^{\infty}(-1)^n B_{sn}\sum_{i=1}^{N}\overline{K}_{xy0}^{i}\cos\lambda_{as}x_{y0}^{i}\cos\lambda_{am}x_{y0}^{i}$$
$$+\sum_{n=0}^{\infty}(-1)^n d_n^1\sum_{i=1}^{N}\overline{K}_{xy0}^{i}\zeta_a^1\left(x_{y0}^{i}\right)\cos\lambda_{am}x_{y0}^{i}$$
$$+\sum_{n=0}^{\infty}(-1)^n d_n^2\sum_{i=1}^{N}\overline{K}_{xy0}^{i}\zeta_a^2\left(x_{y0}^{i}\right)\cos\lambda_{am}x_{y0}^{i} \quad (69)$$
$$=-\overline{\delta}_{am}\sum_{s=0}^{\infty}\sum_{n=0}^{\infty}(-1)^n C_{sn}\lambda_{as}\tau_{am}^{s}$$
$$+\overline{\delta}_{am}\gamma_{1m}\sum_{n=0}^{\infty}(-1)^n f_n^1+\overline{\delta}_{am}\gamma_{2m}\sum_{n=0}^{\infty}(-1)^n f_n^2$$
$$+\overline{\delta}_{am}c_m^2$$

In this paper, all the series expansions have been uniformly truncated to $m = R$ and $n = S$. Equations (58)–(69) can be rewritten in matrix form as

$$HB = QG \tag{70}$$

where

$$H = \begin{bmatrix} H_{1-1} & H_{1-2} & H_{1-3} & H_{1-4} & \cdots & H_{1-12} \\ H_{2-1} & H_{2-2} & H_{2-3} & H_{2-4} & \cdots & H_{2-12} \\ H_{3-1} & H_{3-2} & H_{3-3} & H_{3-4} & \cdots & H_{3-12} \\ H_{4-1} & H_{4-2} & H_{4-3} & H_{4-4} & \cdots & H_{4-12} \\ \vdots & \vdots & \vdots & \vdots & \ddots & \vdots \\ H_{12-1} & H_{12-2} & H_{12-3} & H_{12-4} & \cdots & H_{12-12} \end{bmatrix}$$

$$Q = \begin{bmatrix} Q_{1-1} & Q_{1-2} & Q_{1-3} \\ Q_{2-1} & Q_{2-2} & Q_{2-3} \\ Q_{3-1} & Q_{3-2} & Q_{3-3} \\ Q_{4-1} & Q_{4-2} & Q_{4-3} \\ \vdots & \vdots & \vdots \\ Q_{12-1} & Q_{12-2} & Q_{12-3} \end{bmatrix} \tag{71}$$

$$B = \left\{ \begin{array}{l} a_0^1, a_1^1, \cdots a_M^1, a_0^2, a_1^2 \cdots a_M^2, b_0^1, b_1^1, \cdots b_N^1, b_0^2, b_1^2 \cdots b_N^2, c_0^1, c_1^1, \cdots c_M^1, c_0^2, c_1^2 \cdots c_M^2, \\ d_0^1, d_1^1, \cdots d_N^1, d_0^2, d_1^2 \cdots d_N^2, e_0^1, e_1^1, \cdots e_M^1, e_0^2, e_1^2 \cdots e_M^2, f_0^1, f_1^1, \cdots f_N^1, f_0^2, f_1^2 \cdots f_N^2 \end{array} \right\}^T \tag{72}$$

and

$$G = \left\{ \begin{array}{l} A_{00}, A_{01}, \cdots A_{m'0}, A_{m'1} \cdots A_{m'n'}, \cdots A_{MN}, \\ B_{00}, B_{01}, \cdots B_{m'0}, B_{m'1} \cdots B_{m'n'}, \cdots B_{MN}, \\ B_{00}, B_{01}, \cdots B_{m'0}, B_{m'1} \cdots B_{m'n'}, \cdots B_{MN} \end{array} \right\} \tag{73}$$

All the elements in matrices H and Q can be directly derived from (58)–(69). For example, Appendix B shows the explicit expressions that correspond to the $(n+1)$th equation in (58). Equations (58)–(69) represent $6(R + S + 2)$ linear algebraic equations against a total of $3 \times (R + 1) \times (S + 1) + 6(R+S+2)$ unknown Fourier coefficients. To solve for all these unknowns, additional $3\times(R+1)\times(S+1)$ equations will have to be derived from the governing equations as described below.

2.2. Solving Governing Differential Equations. By substituting (45)–(47) into governing differential equations (1)–(3) and then expanding all the resulting equations and sine functions into cosine series and comparing the like terms, the following equations in matrix form will be deduced:

$$CG + DB + \frac{\rho\omega^2}{\kappa G}(EG + FB) = 0 \tag{74}$$

where

$$C = \begin{bmatrix} C_{1-1} & C_{1-2} & C_{1-3} \\ C_{2-1} & C_{2-2} & C_{2-3} \\ C_{3-1} & C_{3-2} & C_{3-3} \end{bmatrix}$$

$$E = \begin{bmatrix} E_{1-1} & E_{1-2} & E_{1-3} \\ E_{2-1} & E_{2-2} & E_{2-3} \\ E_{3-1} & E_{3-2} & E_{3-3} \end{bmatrix} \tag{75}$$

$$D = \begin{bmatrix} D_{1-1} & D_{1-2} & D_{1-3} & D_{1-4} & \cdots & D_{1-12} \\ D_{2-1} & D_{2-2} & D_{2-3} & D_{2-4} & \cdots & D_{2-12} \\ D_{3-1} & D_{3-2} & D_{3-3} & D_{3-4} & \cdots & D_{3-12} \end{bmatrix} \tag{76}$$

and

$$F = \begin{bmatrix} F_{1-1} & F_{1-2} & F_{1-3} & F_{1-4} & \cdots & F_{1-12} \\ F_{2-1} & F_{2-2} & F_{2-3} & F_{2-4} & \cdots & F_{2-12} \\ F_{3-1} & F_{3-2} & F_{3-3} & F_{3-4} & \cdots & F_{3-12} \end{bmatrix} \tag{77}$$

The elements in the matrices C, D, E, and F can be directly obtained from the results of substitution process. The coefficients in B cannot be treated as independent variables and need to be eliminated from (74) by making use of (70). By doing so, the final characteristic equation can be written as

$$\left(K + \frac{\rho\omega^2}{\kappa G}M\right)A = 0 \tag{78}$$

where $K = C + DH^{-1}Q$ and $M = E + FH^{-1}Q$, and the modal frequencies and the corresponding eigenvectors can now be easily determined by solving a standard matrix eigenproblem. The elements in each eigenvector are actually

Table 1: Frequency parameters $\Omega = \omega b^2(\rho h/D)^{1/2}/\pi^2$ for the square plate of case 1 with restraining stiffness, $\xi_{k_i} = \xi_{Ki} = \xi$, $\xi_{K_{ij}} = 0$, for each point support.

ξ	Method	Model sequence							
		1	2	3	4	5	6	7	8
0	Present	1.2897	1.9201	2.3639	3.2356	3.2356	5.6176	5.6176	5.6459
	FEA	1.2898	1.9212	2.3662	3.2379	3.2379	5.6231	5.6231	5.6522
1	Present	1.2893	1.9204	2.3640	3.2351	3.2351	5.6176	5.6176	5.6447
	FEA	1.2898	1.9216	2.3663	3.2379	3.2379	5.6231	5.6231	5.6522
10^1	Present	1.2919	1.9235	2.3650	3.2363	3.2363	5.6198	5.6198	5.6471
	FEA	1.2898	1.9247	2.3673	3.2385	3.2385	5.6244	5.6244	5.6547
10^2	Present	1.2893	1.9522	2.3741	3.2415	3.2415	5.6322	5.6322	5.6697
	FEA	1.2898	1.9508	2.3756	3.2439	3.2439	5.6364	5.6364	5.6751
10^3	Present	1.2893	2.1249	2.4258	3.2771	3.2771	5.7010	5.7010	5.8077
	FEA	1.2898	2.1093	2.4052	3.2671	3.2671	5.6817	5.6817	5.7570
10^4	Present	1.2898	2.4948	2.4988	3.3767	3.3767	5.8271	5.8271	6.0942
	FEA	1.2898	2.4551	2.4870	3.3610	3.3410	5.8060	5.8060	6.0210
10^6	Present	1.2893	2.4807	2.4889	3.3696	3.3696	5.8123	5.8123	6.0496
	FEA	1.2898	2.4834	2.5011	3.3787	3.3787	5.7769	5.7769	6.0209
10^7	Present	1.2887	1.7945	1.7945	2.1151	2.5149	4.9471	4.9471	6.1398
10^8	Present	1.2887	1.8018	1.8018	2.1325	2.5156	4.9694	4.9694	6.1398
10^9	Present	1.2887	1.8026	1.8026	2.1342	2.5156	4.9716	4.9716	6.1398

the Fourier coefficients for the corresponding mode whose mode shape in the physical space can be simply calculated using (45), (46), (47), and (70).

3. Numerical Examples and Discussion

In this section, some results and discussions about the free vibration of Mindlin rectangular plates are presented to verify the accuracy and flexibility of the proposed method. Based on that, some new results are obtained for Mindlin rectangular plates with various aspect ratios and thicknesses subjected to different point-supported conditions. The discussion is arranged as follows. Firstly, the convergence of the present method is checked when the plate is square rectangular and point-supported. Then, the accuracy of this method is compared with those obtained by FEM commercial program ABAQUS (S4R model). And the following results obtained by FEM are all based on the commercial program ABAQUS (S4R model) unless otherwise stated. In addition, point-supported plates with different geometry parameters and various thicknesses are calculated by the present method. Then, the method is extended to multipoint-supported plate. After the convergence of the multipoint-supported plate is verified, more multipoint-supported plates with different geometry parameters and number of clamped points are calculated through this method.

If not mentioned, the material constants are chosen as follows in this study: $E = 211$ Gpa, $\rho = 7800\,\text{kg/m}^3$, and $\mu = 0.3$. To avoid round-off results, nondimensional frequency is used and stated as follows: $\Omega = \omega b^2(\rho h/D)^{1/2}/\pi^2$. The shear correction factor is selected as $\kappa = 5/6$. In addition, the nondimensional translational, rotational, and torsional springs parameters are defined as $\xi_k = k_i/\gamma$ and $\xi_K = K_i/\varkappa$, $\xi_K = K_{ij}/\varkappa$, where $\gamma = 10^4$ N/m and $\varkappa = 10^4$ N·m/rad.

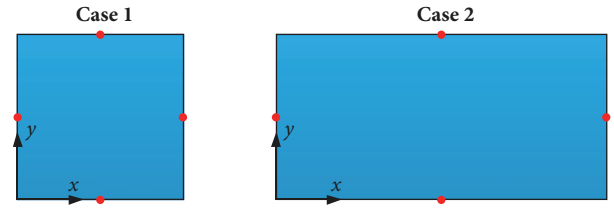

Figure 2: Two-case elastic point support arrangement considered in the calculation.

3.1. Convergence Studies. A Mindlin plate with arbitrary elastic point edge supports is shown in Figure 1. The first example is about point-supported square rectangular plate, namely, case 1 in Figure 2. In Table 1, the first eight nondimensional frequency parameters $\Omega = \omega b^2(\rho h/D)^{1/2}/\pi^2$ for the square plate of case 1 are given with different restraining stiffness ($\xi_{k_i} = \xi_{Ki} = \xi, \xi_{K_{ij}} = 0$) for each point support, and the results are compared with the FEA results. FEA results of Tables 1 and 2 are both obtained by FEM commercial program ABAQUS (S4R model, 18720 elements).

The geometric dimensions of case 1 are as follows: $a = b = 1$ m, $h = 0.1$ m. Besides, series expansion truncated number $R = S = 15$. It is noted that the current results compare well with the FEA results. As shown in Table 1, when nondimensional springs parameters of translational and rotational springs are in the range of $\xi_{k_i} = \xi_{Ki} = 10^7 \sim 10^9$, nondimensional frequency parameter is of convergence. In other words, nondimensional springs parameters at this range can guarantee rigid boundary conditions. When nondimensional springs parameters are less than 10, the boundary conditions can be seen free. To understand the modes of square rectangular plate in free boundary conditions better, the first six mode shapes of square rectangular plates with completely free boundary conditions calculated

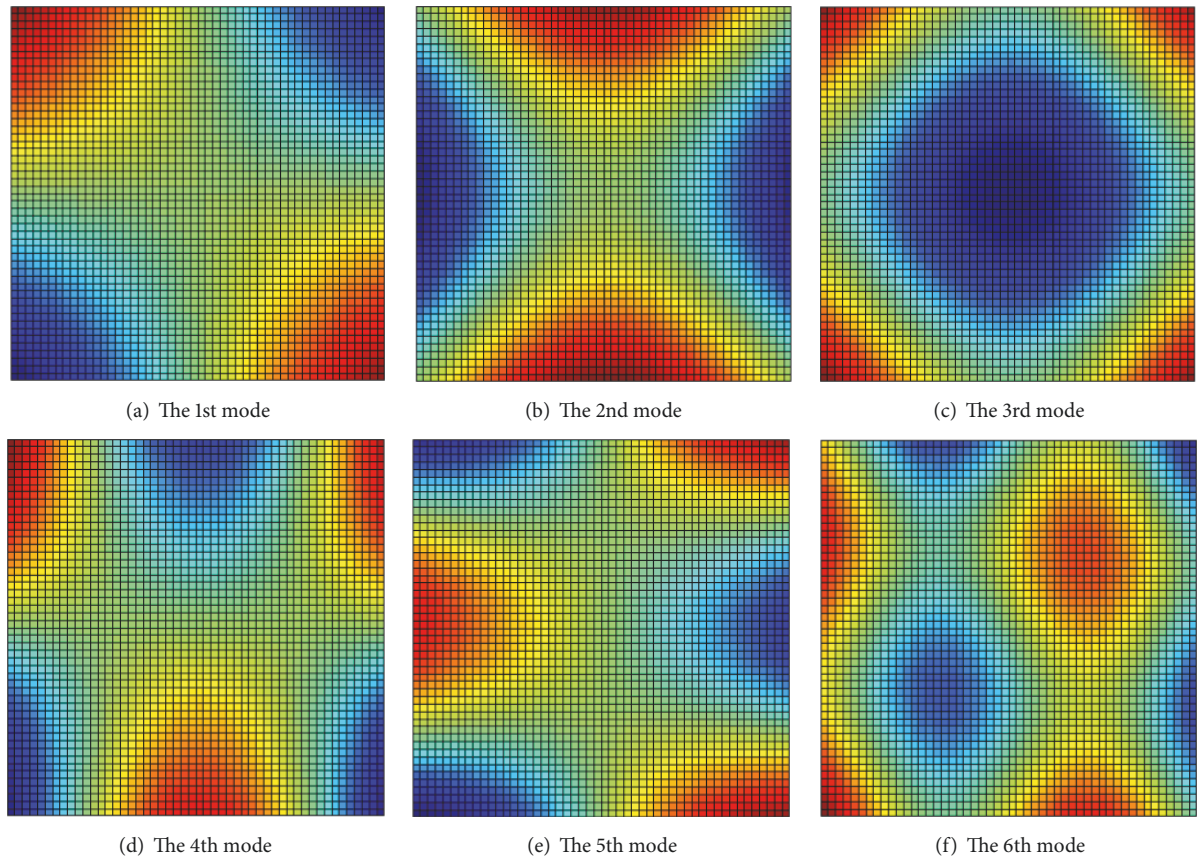

(a) The 1st mode (b) The 2nd mode (c) The 3rd mode

(d) The 4th mode (e) The 5th mode (f) The 6th mode

Figure 3: The first six mode shapes of square rectangular plates with completely free boundary conditions calculated by the present method.

Table 2: Frequency parameters $\Omega = \omega b^2(\rho h/D)^{1/2}/\pi^2$ for the square plate of case 1 with restraining stiffness, $\xi_{k_i} = \xi_{K_i} = 10^4$, $\xi_{K_{ij}} = 0$, for each point support.

R, S	Model sequence							
	1	2	3	4	5	6	7	8
$R = S = 5$	1.2972	2.5625	2.6799	3.4185	3.4185	5.9387	5.9387	6.1675
$R = S = 6$	1.2965	2.5340	2.6052	3.3997	3.3997	5.8960	5.8960	6.1669
$R = S = 7$	1.2919	2.5334	2.6040	3.3969	3.3969	5.8861	5.8861	6.1509
$R = S = 8$	1.2917	2.5164	2.5574	3.3860	3.3860	5.8612	5.8612	6.1305
$R = S = 9$	1.2899	2.5011	2.5562	3.3845	3.3845	5.8561	5.8561	6.1291
$R = S = 10$	1.2898	2.4948	2.4988	3.3767	3.3767	5.8271	5.8271	6.0942
$R = S = 11$	1.2891	2.4796	2.4978	3.3720	3.3720	5.8098	5.8098	6.0657
$R = S = 12$	1.2887	2.4795	2.4877	3.3680	3.3680	5.8096	5.8096	6.0471
$R = S = 13$	1.2887	2.4794	2.4877	3.3679	3.3679	5.8094	5.8094	6.0466
FEA	1.2898	2.4551	2.4870	3.3610	3.3410	5.8060	5.8060	6.0210

by the present method and FEA are presented in Figures 3 and 4. And when the nondimensional springs parameters are in the range of 10^2 and 10^6, the boundary conditions are elastic. As shown in Table 2, the first eight nondimensional frequency parameters become quickly converged at $R = S = 10$ for the given 5-digit precision. For simplicity, the displacement expansion will be truncated to $R = S = 10$ in all the subsequent calculations.

To eliminate the particularity of square rectangular plate, the second example is about point-supported rectangular plate 1b in Figure 2. The geometric dimensions of case 2 are as follows: $a = 2$ m, $b = 1$ m, and $h = 0.1$ m. Besides, series expansion truncated number $R = S = 10$. In Table 3, the first eight nondimensional frequency parameters about 1b calculated by the new method and FEA are given. Meanwhile, the comparison in Table 3 shows the accuracy of the new method to ordinary rectangular Mindlin plate. FEA results of plate 1b in Table 3 and Figure 8 are obtained by FEM commercial program ABAQUS (S4R model, 37500 elements).

3.2. Point-Supported Plate. The accuracy and nice convergence characteristic of this method have been proved when the plate is point-supported. In Table 4, the first eight nondimensional frequency parameters are given with different

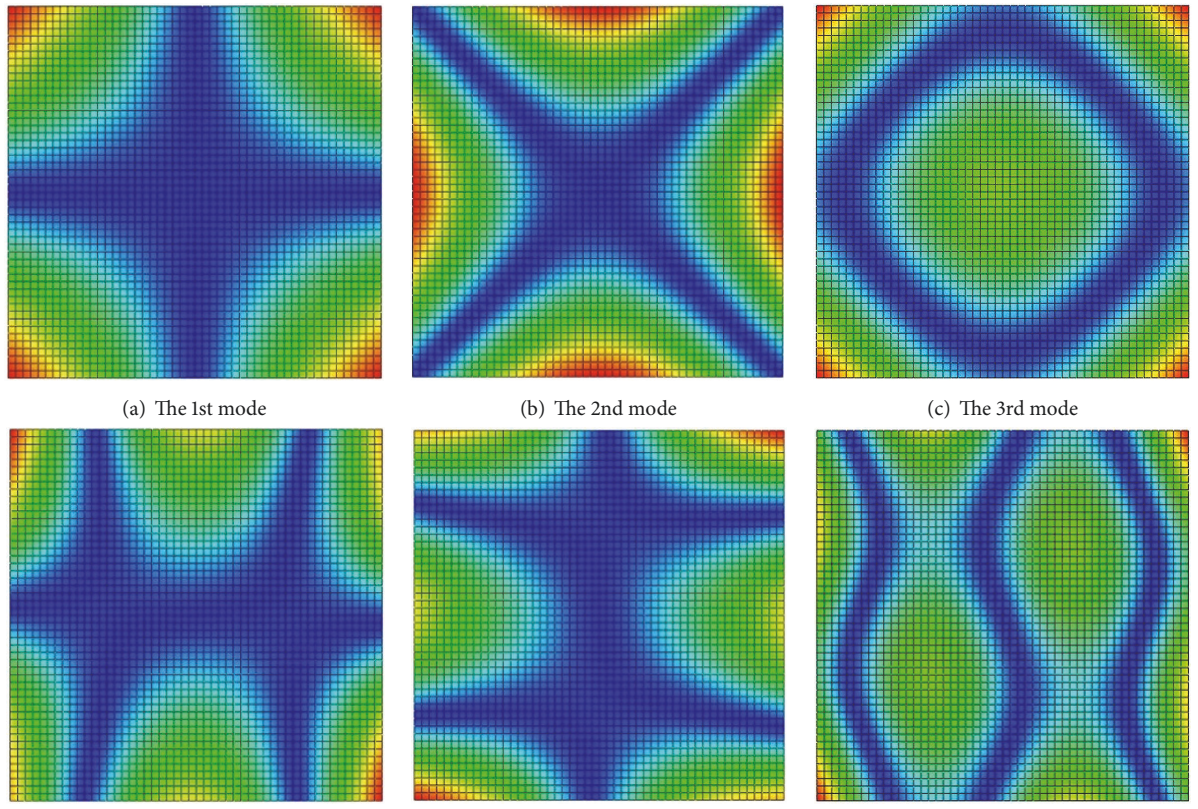

(a) The 1st mode (b) The 2nd mode (c) The 3rd mode

(d) The 4th mode (e) The 5th mode (f) The 6th mode

Figure 4: The first six mode shapes of square rectangular plates with completely free boundary conditions calculated by FEA method.

Table 3: Frequency parameters $\Omega = \omega b^2(\rho h/D)^{1/2}/\pi^2$ for the rectangular plate of case 2 with restraining stiffness, $\xi_{k_i} = \xi_{K_i} = \xi$, $\xi_{K_{ij}} = 0$, for each point support.

ξ	Method	Model sequence							
		1	2	3	4	5	6	7	8
0	Present	0.5383	0.6459	1.4067	1.4669	2.1484	2.4072	2.4924	2.8472
	FEA	0.5396	0.6458	1.4062	1.4685	2.1514	2.4047	2.4948	2.8528
1	Present	0.5387	0.6462	1.4074	1.4677	2.1496	2.4085	2.4937	2.8488
	FEA	0.5388	0.6458	1.4062	1.4687	2.1512	2.4057	2.4948	2.8529
10^1	Present	0.5387	0.6462	1.4074	1.4677	2.1496	2.4085	2.4937	2.8488
	FEA	0.5401	0.6458	1.4067	1.4698	2.1521	2.4057	2.4949	2.8543
10^2	Present	0.5525	0.6462	1.4127	1.4794	2.1593	2.4085	2.4949	2.8633
	FEA	0.5515	0.6458	1.4111	1.4793	2.1599	2.4057	2.4960	2.8661
10^3	Present	0.6283	0.6462	1.4473	1.5438	2.2165	2.4085	2.5031	2.9408
	FEA	0.6045	0.6458	1.4320	1.5171	2.1908	2.4057	2.5019	2.9113
10^4	Present	0.6462	0.8315	1.5615	1.6646	2.3366	2.4085	2.5410	3.0559
	FEA	0.6458	0.8335	1.5597	1.6775	2.3375	2.4057	2.5351	3.0695
10^6	Present	0.6462	0.7899	0.9192	1.1024	1.6561	2.0563	2.4085	2.6004
10^8	Present	0.6462	0.8028	0.9396	1.1561	1.6957	2.0763	2.4085	2.7058
10^{10}	Present	0.6462	0.8043	0.9419	1.1624	1.7001	2.0786	2.4085	2.7180

stiffness values, aspect ratios, and thickness ratios. The first six mode shapes of square rectangular plates with completely elastic boundary conditions ($\xi_{k_i} = \xi_{K_i} = 10^2$, $\xi_{K_{ij}} = 0$) calculated by the present method and FEA are presented in Figures 5 and 6. FEA results of plate 1a in Figure 6 are obtained by FEM commercial program ABAQUS (S4R model, 18720 elements). The first six mode shapes matched well between current method and FEA. It can be seen from Table 4 that nondimensional frequency parameters under elastic boundary conditions tend to decrease with the aspect ratio, whereas the first three modes in each case basically represent the rigid-body motions. The change of these three

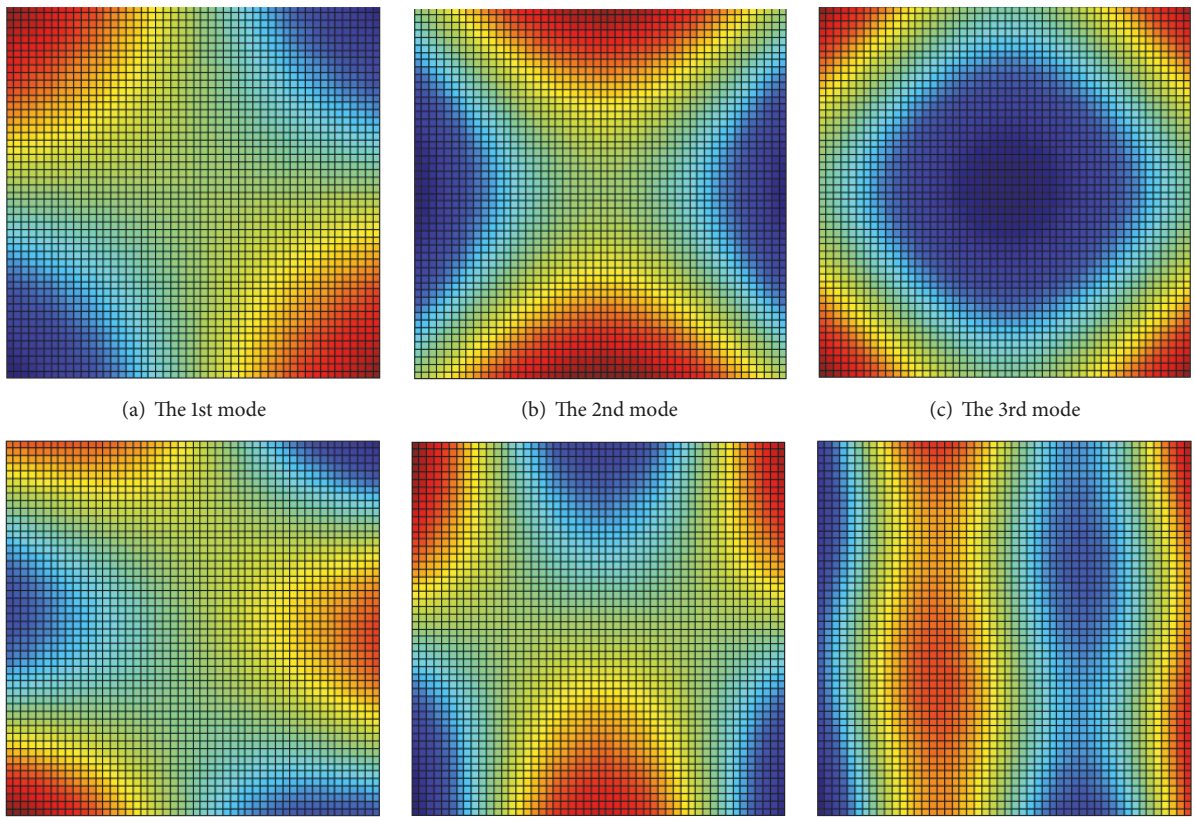

(a) The 1st mode (b) The 2nd mode (c) The 3rd mode

(d) The 4th mode (e) The 5th mode (f) The 6th mode

Figure 5: The first six mode shapes of square rectangular plates with completely elastic boundary conditions, $\xi_{k_i} = \xi_{K_i} = 10^2$, $\xi_{K_{ij}} = 0$, calculated by the present method.

Table 4: Frequency parameters $\Omega = \omega b^2(\rho h/D)^{1/2}/\pi^2$ for the restraining stiffness point support plate with different geometry parameters, $\xi_{k_i} = \xi_{K_i} = \xi$, $\xi_{K_{ij}} = 0$, for each point support.

ξ	a/b	h/b	Model sequence							
			1	2	3	4	5	6	7	8
10^2	$a/b = 1$	$h/b = 0.1$	1.2890	1.9514	2.3730	3.2405	3.2405	5.6196	5.6196	5.6683
		$h/b = 0.2$	1.1847	1.7660	2.1468	2.7913	2.7913	4.5648	4.5766	4.5766
	$a/b = 2$	$h/b = 0.1$	0.5522	0.6459	1.4120	1.4786	2.1582	2.4072	2.4936	2.8618
		$h/b = 0.2$	0.5257	0.6078	1.2908	1.3669	1.9617	2.1320	2.2271	2.5177
	$a/b = 5$	$h/b = 0.1$	0.4743	0.5256	0.7779	0.8091	1.1345	1.1556	1.4961	1.6006
		$h/b = 0.2$	0.4572	0.4914	0.7426	0.7581	1.0495	1.0856	1.3696	1.4769
10^4	$a/b = 1$	$h/b = 0.1$	1.2890	2.4948	2.4988	3.3720	3.3720	5.8218	5.8218	6.0670
		$h/b = 0.2$	1.1847	1.9651	2.1982	2.8358	2.8358	4.6511	4.6511	4.7226
	$a/b = 2$	$h/b = 0.1$	0.6459	0.8311	1.5607	1.6637	2.3354	2.4072	2.5397	3.0544
		$h/b = 0.2$	0.6078	0.6183	1.3357	1.4389	2.0232	2.1320	2.2380	2.6037
	$a/b = 5$	$h/b = 0.1$	0.3967	0.6293	0.6891	0.8091	0.8794	1.2422	1.2678	1.4961
		$h/b = 0.2$	0.2805	0.5012	0.5478	0.7581	0.7766	1.0786	1.1222	1.3696
10^6	$a/b = 1$	$h/b = 0.1$	1.2890	1.7336	1.7336	1.9936	2.5169	4.7623	4.7623	5.6910
		$h/b = 0.2$	1.1585	1.1763	1.1763	1.1847	2.2452	3.2096	3.3393	3.3393
	$a/b = 2$	$h/b = 0.1$	0.6459	0.7895	0.9188	1.1018	1.6552	2.0553	2.4072	2.5990
		$h/b = 0.2$	0.6078	0.6419	0.7129	0.7410	1.2653	1.7296	1.8630	2.1320
	$a/b = 5$	$h/b = 0.1$	0.1945	0.2536	0.2787	0.2843	0.6492	0.7673	0.8091	0.8821
		$h/b = 0.2$	0.1807	0.2407	0.2524	0.2540	0.5723	0.6156	0.7581	0.7802

Table 5: Frequency parameters $\Omega = \omega b^2(\rho h/D)^{1/2}/\pi^2$ for the multipoint-supported square plate; the numbers of clamped points is 26 on every edge.

R, S	Model sequence							
	1	2	3	4	5	6	7	8
$R = S = 6$	3.2837	6.2606	6.2606	8.7450	10.3330	10.4515	12.4545	12.4545
$R = S = 7$	3.2835	6.2569	6.2569	8.7372	10.3311	10.4495	12.4501	12.4501
$R = S = 8$	3.2826	6.2562	6.2562	8.7369	10.3221	10.4411	12.4411	12.4411
$R = S = 9$	3.2823	6.2552	6.2552	8.7349	10.3218	10.4408	12.4400	12.4400
$R = S = 10$	3.2823	6.2550	6.2550	8.7348	10.3201	10.4386	12.4376	12.4376
$R = S = 12$	3.2823	6.2550	6.2550	8.7348	10.3194	10.4386	12.4375	12.4375
$R = S = 14$	3.2823	6.2550	6.2550	8.7348	10.3194	10.4386	12.4375	12.4375
CC1	3.2870	6.2578	6.2578	8.7352	10.3247	10.4418	12.4412	12.4412

∗CC1 refers to the uniformly clamped plate with $a/b = 1$, $h/b = 0.1$ and calculated by ABAQUS.

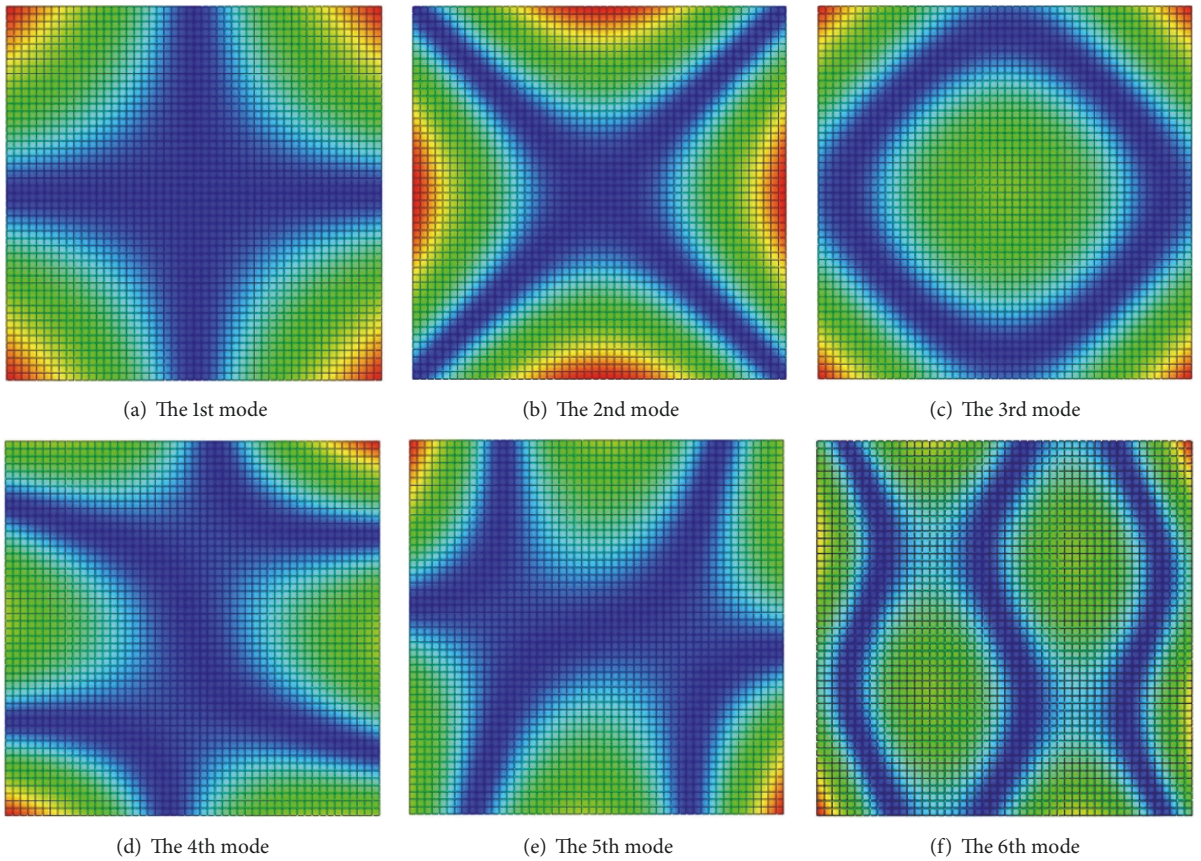

(a) The 1st mode (b) The 2nd mode (c) The 3rd mode

(d) The 4th mode (e) The 5th mode (f) The 6th mode

Figure 6: The first six mode shapes of square rectangular plates with completely elastic boundary conditions, $\xi_{k_i} = \xi_{K_i} = 10^2$, $\xi_{K_{ij}} = 0$, calculated by FEA method.

modes is smaller than higher modes. With the increase of nondimensional spring parameters, the boundary conditions change from elastic to clamped. When the spring stiffness is set as $\xi_{k_i} = \xi_{K_i} = 10^8$, $\xi_{K_{ij}} = 0$, the first six mode shapes of 1a and 1b which are displayed in Figures 7 and 8 can be seen as point clamped.

3.3. Multipoint-Supported Plate. It is proved that the present method is convergent and accurate when the plate is point-supported from the previous study. In this subsection, nondimensional frequency parameters $\Omega = \omega b^2(\rho h/D)^{1/2}/\pi^2$ of the multipoint-supported square plate 1a ($a = 1$ m, $b = 1$ m, and $h = 0.1$ m) with different numbers of terms in the series expansion (R and S) are shown in Table 5. The nondimensional spring parameters translational and rotational springs are set as 10^8 N/m and 10^8 N·m/rad, respectively; besides, there are 26 clamped points on every edge. This shows that the results are very accurate when R and S are small numbers. When truncated numbers R and S are larger than 10, results are almost invariant. The displacement expansion will be truncated to $R = S = 10$ in the subsequent calculations of multipoint-supported plate. For the lack of relevant literature,

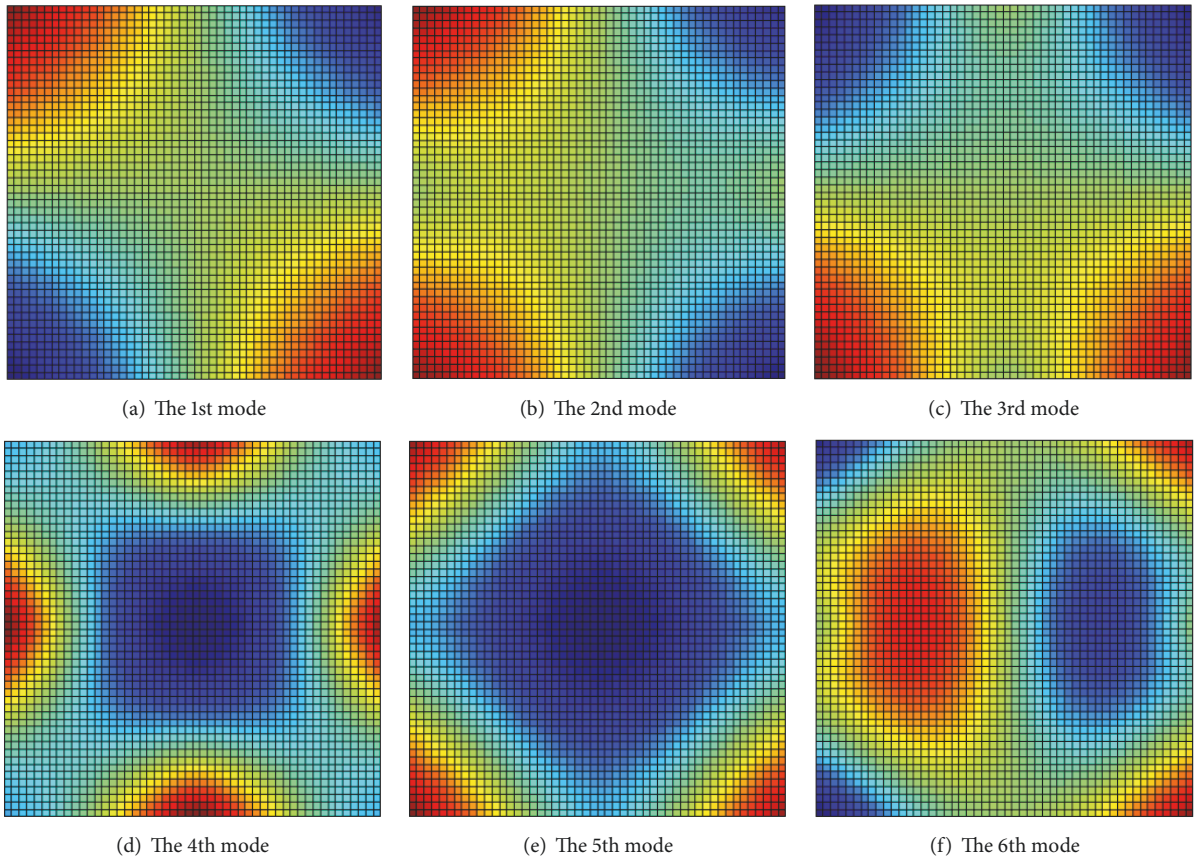

(a) The 1st mode (b) The 2nd mode (c) The 3rd mode

(d) The 4th mode (e) The 5th mode (f) The 6th mode

FIGURE 7: The first six mode shapes of square rectangular plates with completely elastic boundary conditions, $\xi_{k_i} = \xi_{K_i} = 10^8$, $\xi_{K_{ij}} = 0$, calculated by the present method.

the FEM data is given as a comparison. The FEM data is obtained through ABAQUS (S4R); each edge is divided into 100 pieces, which is considered adequately fine to capture the spatial variations of these lower order modes. Besides, the mode shapes calculated through FEM are displayed in Figure 10. The first six mode shapes of square rectangular plates with 26 clamped points on every edge which are calculated by the present method are presented in Figure 9. Both nondimensional frequency and mode shapes of square rectangular plate matched well between the new method and FEA. The accuracy and nice convergence characteristic of this method have been proved when the plate is multipoint-supported.

In Table 6, the first eight nondimensional frequency parameters are given with different number of clamped points, aspect ratios, and thickness ratios. Similarly, nondimensional frequency parameters tend to decrease with the aspect ratio when the plate is multipoint-supported.

Figure 11 shows the difference of nondimensional frequency parameters between different numbers of clamped points and clamped boundary condition, in which three kinds of aspect ratios and thickness ratios are considered. The first three frequency parameters of multipoints plate and clamped plate are, respectively, calculated by the current method and ABAQUS. With the increase of the number of clamped points on each edge, the percentage error between multipoints plate and clamped plate narrows quickly. When the number of clamped points is bigger than 16 at each edge, the discrepancy between nondimensional frequency parameters of multipoints plate and clamped plate is tiny and invariant. The maximum percentage error is 0.31%, which means multipoints boundary condition is equal to clamped boundary condition.

Based on different plate theories, the first frequency and error of multipoint clamped square plates with different thickness ratios and number of clamped points are listed in Figure 12. The error is defined as $Error(\%) = |\Omega_\alpha - \Omega_{3D}|/\Omega_{3D} \times 100\%$, in which α represents classical plate theory, Mindlin plate theory, and three-dimensional (3D) elastic theory, respectively. It is easy to find that classical thin plate theory overestimates the plate frequencies for the neglect of transverse shear and rotary inertia. The discrepancy of thin plates using Mindlin and classical plate theory is tiny to neglect when the thickness ratio is less than 0.05. However, the error of classical plate theory increases rapidly when the thickness ratio is more than 0.1 and is generally more than 10%. Meanwhile, the error of Mindlin plate theory is only 1.1% when the thickness ratio is 0.2. The introduction of Mindlin theory is necessary when the plate is not a thin plate (thickness ratio is less than 0.1).

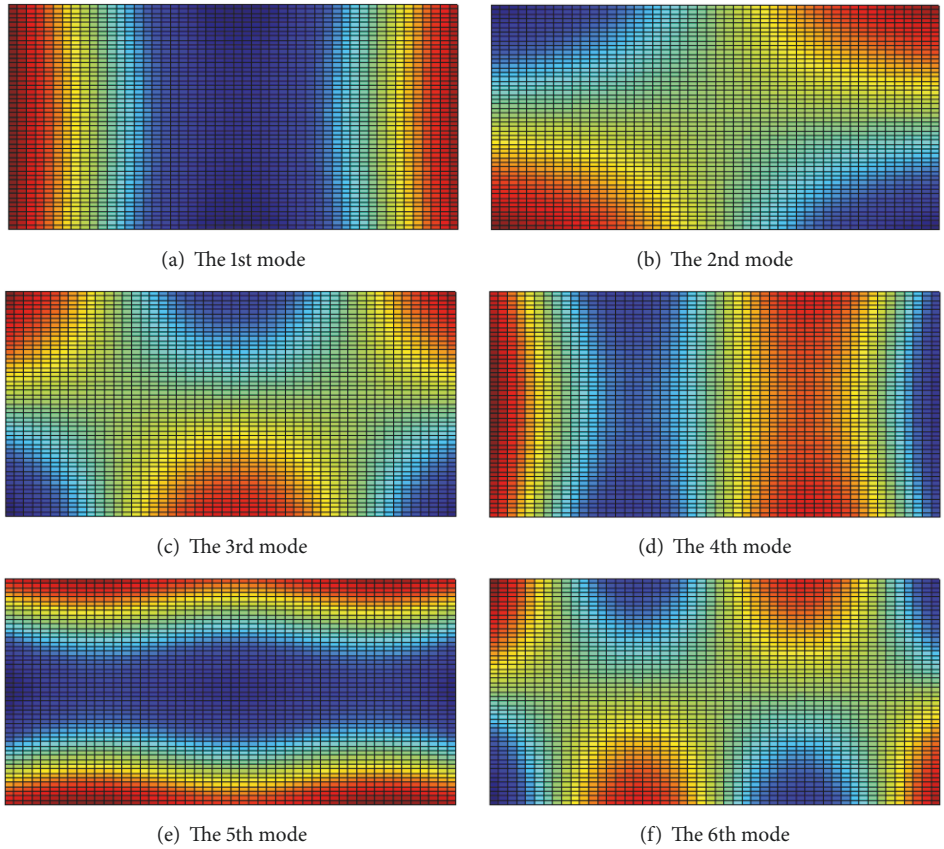

(a) The 1st mode (b) The 2nd mode

(c) The 3rd mode (d) The 4th mode

(e) The 5th mode (f) The 6th mode

FIGURE 8: The first six mode shapes of rectangular plates with completely elastic boundary conditions and the aspect ratio as $a/b = 2$, $h/b = 0.1$, $\xi_{k_i} = \xi_{K_i} = 10^8$, and $\xi_{K_{ij}} = 0$, calculated by the present method.

4. Conclusions

In this paper, a modified Fourier method has been presented to study the free vibration behaviors of moderately thick rectangular plates with different point-supported conditions. The first-order shear deformation plate theory is adopted to formulate the theoretical model. The displacement and rotation fields of plates, regardless of boundary conditions, are generally sought as a new form of trigonometric series expansions in which several supplementary closed functions are introduced to ensure and accelerate the convergence of the series expansion. Not only is the series expansion representation of solution applicable to any boundary conditions, but also the convergence of the series expansion can be substantially improved. Rayleigh–Ritz method is employed to obtain solution by the energy description of the plates. The convergence of the present solution is examined and the excellent accuracy is validated by comparison with FEM data. Excellent agreements are obtained from these comparisons. The proposed method provides a unified means for extracting the modal parameters and predicting the vibration behaviors of moderately thick plates with arbitrary point-supported edge restraints. A variety of free vibration results for moderately thick rectangular plates with different aspect ratios, thickness ratios, and boundary conditions are presented. From the results in this paper, we can find that nondimensional frequency tends to decrease with the aspect ratio, whereas the change of these three modes is smaller than higher modes under elastic boundary conditions. In addition, with the increase of the number of clamped points on edge of rectangular plate, the boundary condition converges to fully clamped edge condition. Finally, we have verified that classical thin plate theory overestimates the plate frequencies for the neglect of transverse shear and rotary inertia. It is necessary to introduce Mindlin theory when considering the vibration of moderately thick plate.

Appendix

A. The Expressions for Fourier Cosine Expansion Coefficient

$$\zeta_a^1(x) = \frac{a}{2\pi}\sin\left(\frac{\pi x}{2a}\right) + \frac{a}{2\pi}\sin\left(\frac{3\pi x}{2a}\right) = \sum_{m=0}^{\infty}\alpha_{1m}\cos\lambda_{am}x \tag{A.1}$$

$$\alpha_{1m} = \begin{cases} \dfrac{4a}{3\pi^2} & m = 0 \\ \dfrac{2a}{(1-4m^2)\pi^2} + \dfrac{6a}{(9-4m^2)\pi^2} & m \neq 0 \end{cases}$$

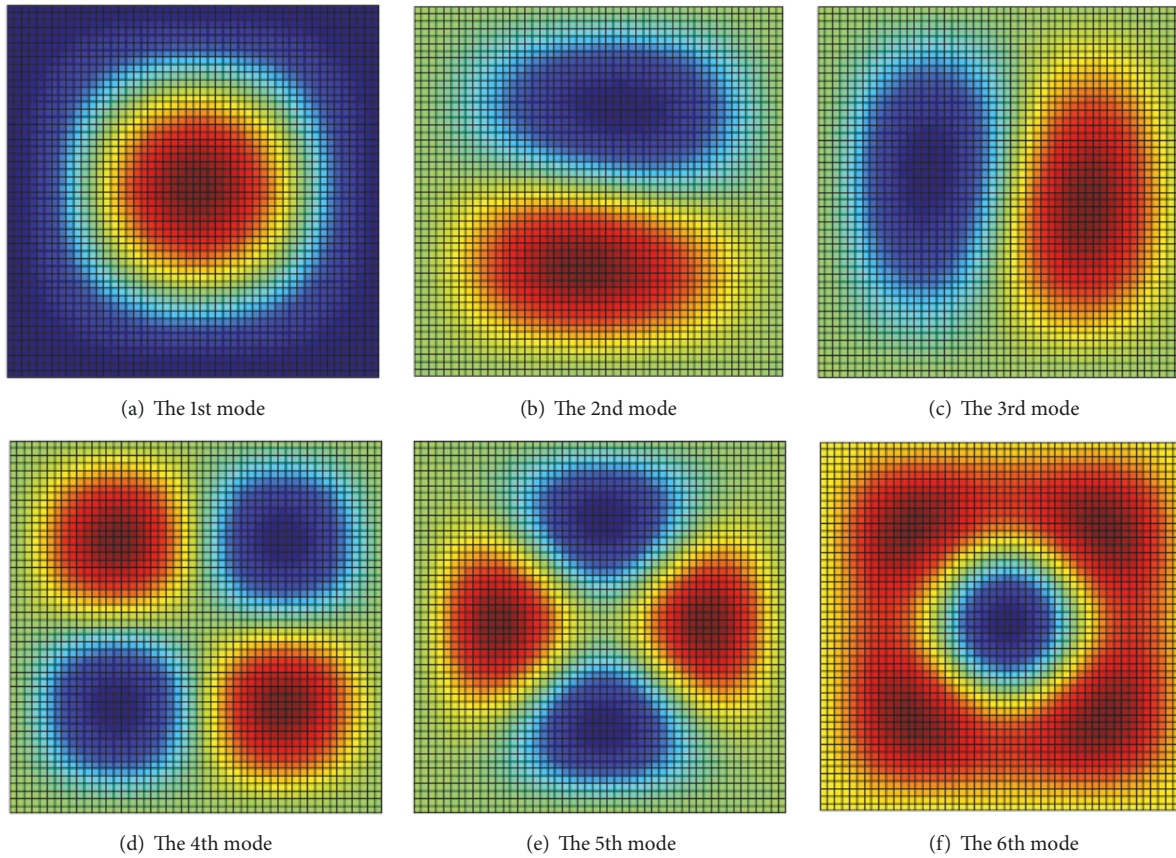

(a) The 1st mode (b) The 2nd mode (c) The 3rd mode

(d) The 4th mode (e) The 5th mode (f) The 6th mode

Figure 9: The first six mode shapes of square rectangular plates with multipoint support, calculated by the present method.

$$\zeta_a^2(x) = -\frac{a}{2\pi}\sin\left(\frac{\pi x}{2a}\right) + \frac{a}{2\pi}\sin\left(\frac{3\pi x}{2a}\right) = \sum_{m=0}^{\infty}\alpha_{2m}\cos\lambda_{am}x \tag{A.2}$$

$$\alpha_{2m} = \begin{cases} -\dfrac{2a}{3\pi^2} & m = 0 \\ -\dfrac{2a(-1)^m}{(1-4m^2)\pi^2} + \dfrac{6a(-1)^{m+1}}{(9-4m^2)\pi^2} & m \neq 0 \end{cases}$$

$$\zeta_b^1(y) = \frac{b}{2\pi}\sin\left(\frac{\pi y}{2b}\right) + \frac{b}{2\pi}\sin\left(\frac{3\pi y}{2b}\right) = \sum_{n=0}^{\infty}\beta_{1n}\cos\lambda_{bn}y \tag{A.3}$$

$$\beta_{1n} = \begin{cases} \dfrac{4b}{3\pi^2} & n = 0 \\ \dfrac{2b}{(1-4n^2)\pi^2} + \dfrac{6b}{(9-4n^2)\pi^2} & n \neq 0 \end{cases}$$

$$\zeta_b^2(y) = -\frac{b}{2\pi}\sin\left(\frac{\pi y}{2b}\right) + \frac{b}{2\pi}\sin\left(\frac{3\pi y}{2b}\right) = \sum_{n=0}^{\infty}\beta_{2n}\cos\lambda_{bn}y$$

$$\beta_{2n} = \begin{cases} -\dfrac{2b}{3\pi^2} & n = 0 \\ -\dfrac{2b(-1)^n}{(1-4n^2)\pi^2} + \dfrac{6b(-1)^{n+1}}{(9-4n^2)\pi^2} & n \neq 0 \end{cases} \tag{A.4}$$

$$\zeta_a^{1'}(x) = \frac{1}{4}\cos\left(\frac{\pi x}{2a}\right) + \frac{3}{4}\cos\left(\frac{3\pi x}{2a}\right) = \sum_{m=0}^{\infty}\gamma_{1m}\cos\lambda_{am}x \tag{A.5}$$

$$\gamma_{1m} = \begin{cases} \dfrac{1}{\pi} & m = 0 \\ \dfrac{(-1)^m}{(1-4m^2)\pi} + \dfrac{9(-1)^{m+1}}{(9-4m^2)\pi} & m \neq 0 \end{cases}$$

$$\zeta_a^{2'}(x) = \frac{1}{4}\sin\left(\frac{\pi x}{2a}\right) - \frac{3}{4}\sin\left(\frac{3\pi x}{2a}\right) = \sum_{m=0}^{\infty}\gamma_{2m}\cos\lambda_{am}x \tag{A.6}$$

$$\gamma_{2m} = \begin{cases} 0 & m = 0 \\ \dfrac{1}{(1-4m^2)\pi} - \dfrac{9}{(9-4m^2)\pi} & m \neq 0 \end{cases}$$

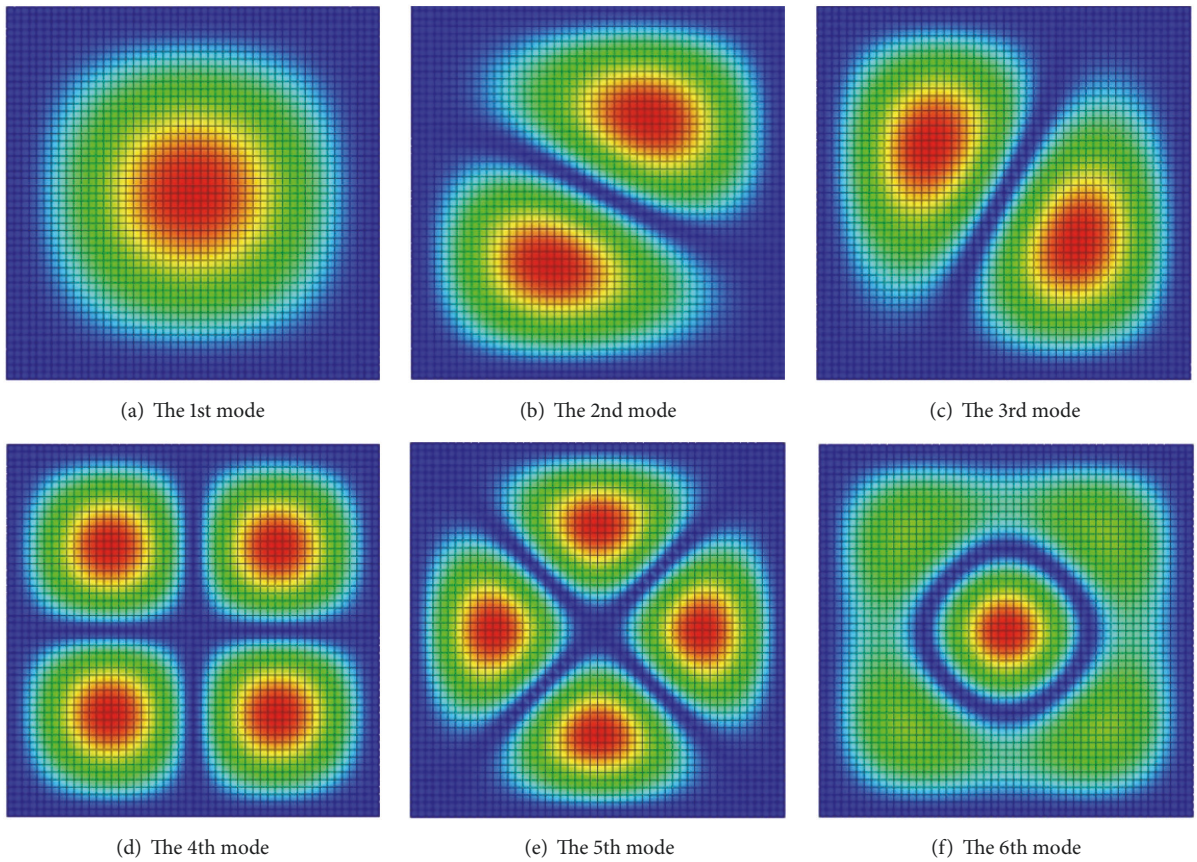

(a) The 1st mode (b) The 2nd mode (c) The 3rd mode

(d) The 4th mode (e) The 5th mode (f) The 6th mode

Figure 10: The first six mode shapes of square rectangular plates with uniform completely clamped boundary conditions, calculated by FEA method.

$$\zeta_b^{1'}(y) = \frac{1}{4}\cos\left(\frac{\pi y}{2b}\right) + \frac{3}{4}\cos\left(\frac{3\pi y}{2b}\right) = \sum_{n=0}^{\infty}\eta_{1n}\cos\lambda_{bn}y$$

$$\eta_{1n} = \begin{cases} \frac{1}{\pi} & n = 0 \\ \frac{(-1)^n}{(1-4n^2)\pi} + \frac{9(-1)^{n+1}}{(9-4n^2)\pi} & n \neq 0 \end{cases} \tag{A.7}$$

$$\zeta_b^{2'}(x) = \frac{1}{4}\sin\left(\frac{\pi y}{2b}\right) - \frac{3}{4}\sin\left(\frac{3\pi y}{2b}\right) = \sum_{n=0}^{\infty}\eta_{2n}\cos\lambda_{bn}y$$

$$\eta_{2n} = \begin{cases} 0 & n = 0 \\ \frac{1}{(1-4n^2)\pi} - \frac{9}{(9-4n^2)\pi} & n \neq 0 \end{cases} \tag{A.8}$$

$$\zeta_a^{1''}(x) = -\frac{\pi}{8a}\sin\left(\frac{\pi x}{2a}\right) - \frac{9\pi}{8a}\sin\left(\frac{3\pi x}{2a}\right) = \sum_{m=0}^{\infty}\phi_{1m}\cos\lambda_{am}x$$

$$\phi_{1m} = \begin{cases} -\frac{1}{a} & m = 0 \\ -\frac{1}{2(1-4m^2)a} - \frac{27}{2(9-4m^2)a} & m \neq 0 \end{cases} \tag{A.9}$$

$$\zeta_a^{2''}(x) = \frac{\pi}{8a}\cos\left(\frac{\pi x}{2a}\right) - \frac{9\pi}{8a}\cos\left(\frac{3\pi x}{2a}\right) = \sum_{m=0}^{\infty}\phi_{2m}\cos\lambda_{am}x$$

$$\phi_{2m} = \begin{cases} -\frac{1}{2a} & m = 0 \\ \frac{(-1)^m}{2(1-4m^2)a} - \frac{27(-1)^{m+1}}{2(9-4m^2)a} & m \neq 0 \end{cases} \tag{A.10}$$

$$\zeta_b^{1''}(y) = -\frac{\pi}{8a}\sin\left(\frac{\pi y}{2b}\right) - \frac{9\pi}{8a}\sin\left(\frac{3\pi y}{2b}\right) = \sum_{n=0}^{\infty}\varphi_{1n}\cos\lambda_{bn}y$$

$$\varphi_{1n} = \begin{cases} -\frac{1}{b} & n = 0 \\ -\frac{1}{2(1-4n^2)a} - \frac{27}{2(9-4n^2)a} & n \neq 0 \end{cases} \tag{A.11}$$

Table 6: Frequency parameters $\Omega = \omega b^2(\rho h/D)^{1/2}/\pi^2$ for the multipoint-supported plate with different geometry parameters and numbers of clamped points.

geometry parameters	No. of clamped points	Model sequence							
		1	2	3	4	5	6	7	8
$a/b = 3$, $h/b = 0.1$	4	1.5833	1.6832	2.0553	2.0597	2.4456	2.7332	3.0820	3.1456
	8	2.1798	2.4123	2.6437	3.2877	4.1133	5.1177	5.4172	5.5959
	12	2.1833	2.4178	2.8495	3.4943	4.3430	5.3744	5.4539	5.6759
	16	2.1834	2.4181	2.8503	3.4958	4.3451	5.3773	5.4542	5.6769
	20	2.1834	2.4181	2.8503	3.4958	4.3451	5.3773	5.4542	5.6769
	22	2.1834	2.4181	2.8503	3.4958	4.3451	5.3773	5.4542	5.6769
	26	2.1834	2.4181	2.8503	3.4958	4.3451	5.3773	5.4542	5.6769
	28	2.1834	2.4181	2.8503	3.4958	4.3451	5.3773	5.4542	5.6769
	30	2.1834	2.4181	2.8503	3.4958	4.3451	5.3773	5.4542	5.6769
	CC1	2.1810	2.4181	2.8536	3.4987	4.3445	5.3795	5.4602	5.6776
$a/b = 3$, $h/b = 0.2$	4	1.3105	1.4309	1.6865	1.7451	2.1095	2.1927	2.3602	2.4646
	8	1.8389	2.0139	2.1817	2.6793	3.2958	4.0280	4.0619	4.1648
	12	1.8424	2.0205	2.3551	2.8496	3.4791	4.1086	4.2146	4.2583
	16	1.8426	2.0212	2.3569	2.8521	3.4824	4.1089	4.2180	4.2592
	20	1.8426	2.0212	2.3569	2.8521	3.4824	4.1089	4.2180	4.2592
	22	1.8426	2.0212	2.3569	2.8521	3.4824	4.1089	4.2180	4.2592
	26	1.8426	2.0212	2.3569	2.8521	3.4824	4.1089	4.2180	4.2592
	28	1.8426	2.0212	2.3569	2.8521	3.4824	4.1089	4.2180	4.2592
	30	1.8426	2.0212	2.3569	2.8521	3.4824	4.1089	4.2180	4.2592
	CC2	1.8449	2.0268	2.3604	2.8596	3.4840	4.1151	4.2190	4.2672
$a/b = 5$, $h/b = 0.2$	4	0.6581	0.8020	0.9433	0.9906	1.1117	1.1914	1.3123	1.4223
	8	1.6839	1.7695	1.8092	1.8715	1.9115	2.0716	2.5176	2.5228
	12	1.8057	1.8566	1.9511	2.0984	2.3047	2.5709	2.8942	3.2685
	16	1.8058	1.8571	1.9521	2.1004	2.3074	2.5745	2.8979	3.2729
	20	1.8058	1.8571	1.9521	2.1004	2.3074	2.5745	2.8979	3.2729
	22	1.8058	1.8571	1.9521	2.1004	2.3074	2.5745	2.8979	3.2729
	26	1.8058	1.8571	1.9521	2.1004	2.3074	2.5745	2.8979	3.2729
	28	1.8058	1.8571	1.9521	2.1004	2.3074	2.5745	2.8979	3.2729
	30	1.8058	1.8571	1.9521	2.1004	2.3074	2.5745	2.8979	3.2729
	CC3	1.8097	1.8629	1.9553	2.1043	2.3078	2.5626	2.9013	3.2779

∗CC1: refers to the uniformly clamped plate with $a/b = 3$, $h/b = 0.1$ and calculated by ABAQUS. CC2: refers to the uniformly clamped plate with $a/b = 3$, $h/b = 0.2$ and calculated by ABAQUS. CC3: refers to the uniformly clamped plate with $a/b = 5$, $h/b = 0.2$ and calculated by ABAQUS.

$$\zeta_b^{2''}(y) = \frac{\pi}{8b}\cos\left(\frac{\pi y}{2b}\right) - \frac{9\pi}{8b}\cos\left(\frac{3\pi y}{2b}\right) = \sum_{n=0}^{\infty}\varphi_{2n}\cos\lambda_{bn}y$$

$$\varphi_{2n} = \begin{cases} -\dfrac{1}{2b} & n = 0 \\ \dfrac{(-1)^n}{2\left(1-4n^2\right)b} - \dfrac{27\,(-1)^{n+1}}{2\left(9-4n^2\right)b} & n \neq 0 \end{cases} \tag{A.12}$$

$$\sin\lambda_{am}x = \sum_{p}^{\infty}\tau_{ap}^{m}\cos\lambda_{ap}x = \sin\lambda_{ap}x = \sum_{m=0}^{\infty}\tau_{am}^{p}\cos\lambda_{am}x$$

$$\tau_{am}^{p} = 0 \quad p = 0$$

$$\tau_{am}^{p} = \begin{cases} m = 0 & \dfrac{1-(-1)^p}{p\pi} \\ m \neq 0 & \begin{cases} m = p & 0 \\ m \neq p & \dfrac{2p\left[(-1)^{m+p}-1\right]}{\left(m^2-p^2\right)\pi} \end{cases} \end{cases} \quad p \neq 0 \tag{A.13}$$

$$\sin\lambda_{bn}y = \sum_{q}^{\infty}\tau_{bq}^{n}\cos\lambda_{bq}y = \sin\lambda_{bq}x = \sum_{n=0}^{\infty}\tau_{bn}^{q}\cos\lambda_{bn}y$$

$$\tau_{bn}^{q} = 0 \quad q = 0$$

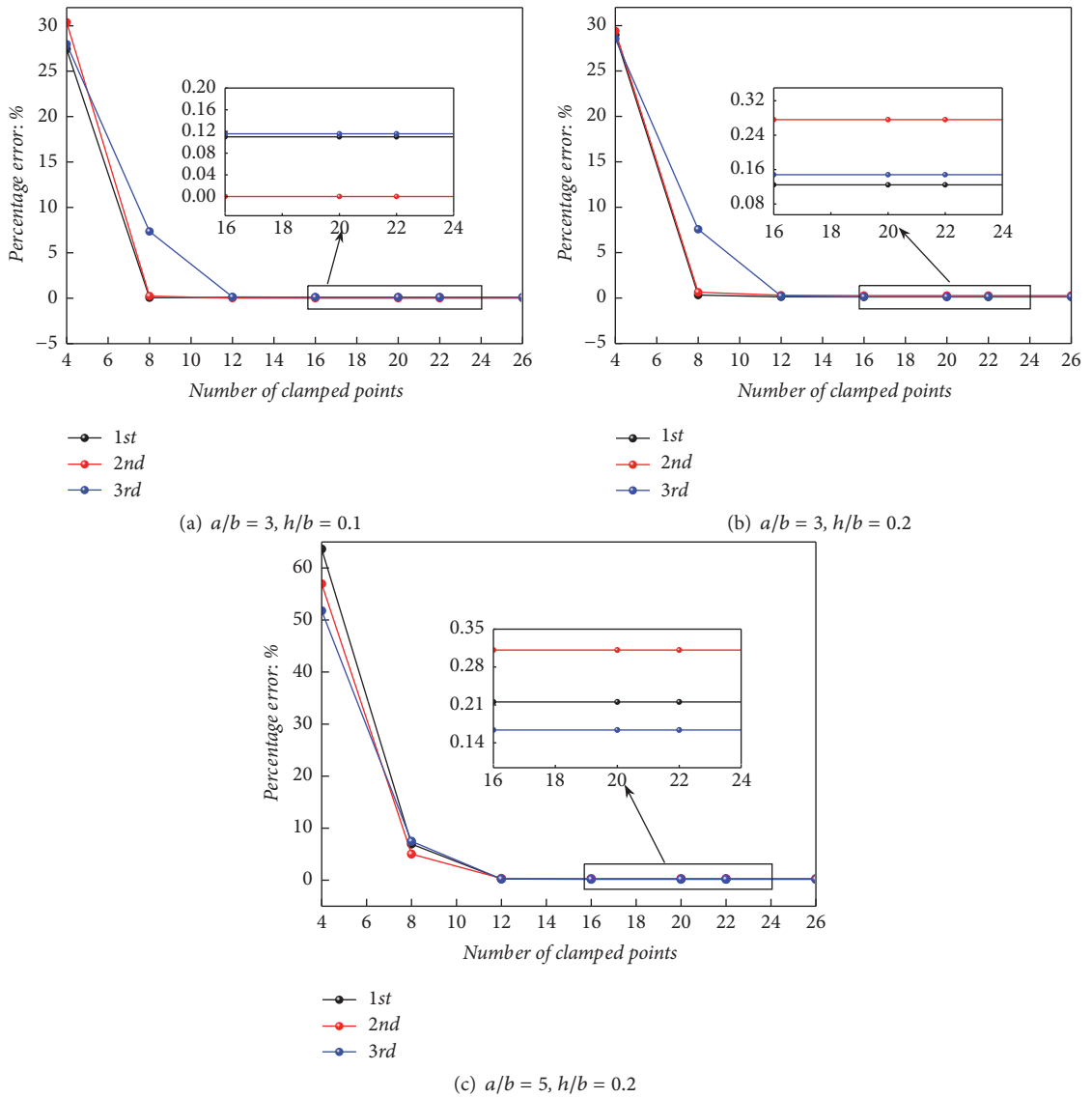

(a) $a/b = 3$, $h/b = 0.1$

(b) $a/b = 3$, $h/b = 0.2$

(c) $a/b = 5$, $h/b = 0.2$

FIGURE 11: The discrepancy of nondimensional frequency parameters between different numbers of clamped points and clamped boundary condition ($b = 1$ m).

$$\tau_{bn}^{q} = \begin{cases} n = 0 & \dfrac{1-(-1)^{q}}{q\pi} \\ n \neq 0 & \begin{cases} n = q & 0 \\ n \neq q & \dfrac{2q\left[(-1)^{n+q}-1\right]}{\left(n^{2}-q^{2}\right)\pi} \end{cases} \end{cases} \quad q \neq 0 \tag{A.14}$$

B. The Explicit Expressions Corresponding to the $(n+1)th$ Equation in (58)

$$\{H_{1-1}\}_{n+1,m'+1} = \sum_{i=1}^{N} \overline{k}_{x0}^{i} \zeta_{b}^{1}\left(y_{x0}^{i}\right) \cos \lambda_{bn} y_{x0}^{i} \tag{B.1}$$

$$\{H_{1-2}\}_{n+1,m+1} = \sum_{i=1}^{N} \overline{k}_{x0}^{i} \zeta_{b}^{2}\left(y_{x0}^{i}\right) \cos \lambda_{bn} y_{x0}^{i} \tag{B.2}$$

$$\{H_{1-3}\}_{n+1,n'+1} = \overline{\delta}_{bn}\delta_{nn'} \tag{B.3}$$

$$\{H_{1-4}\}_{n+1,n'+1} = 0 \tag{B.4}$$

$$\{H_{1-5}\}_{n+1,m'+1} = -\overline{\delta}_{bn}\beta_{1n} \tag{B.5}$$

$$\{H_{1-6}\}_{n+1,m'+1} = -\overline{\delta}_{bn}\beta_{2n} \tag{B.6}$$

$$\{H_{1-7}\}_{n+1,n'+1} = \{H_{1-8}\}_{n+1,n'+1} = 0 \tag{B.7}$$

$$\{H_{1-9}\}_{n+1,m'+1} = \{H_{1-10}\}_{n+1,m'+1} = 0 \tag{B.8}$$

$$\{H_{1-11}\}_{n+1,n'+1} = \{H_{1-12}\}_{n+1,n'+1} = 0 \tag{B.9}$$

$$\{Q_{1-1}\}_{n+1,t} = \sum_{i=1}^{N} \overline{k}_{x0}^{i} \cos \lambda_{bt} y_{x0}^{i} \cos \lambda_{bn} y_{x0}^{i} \tag{B.10}$$

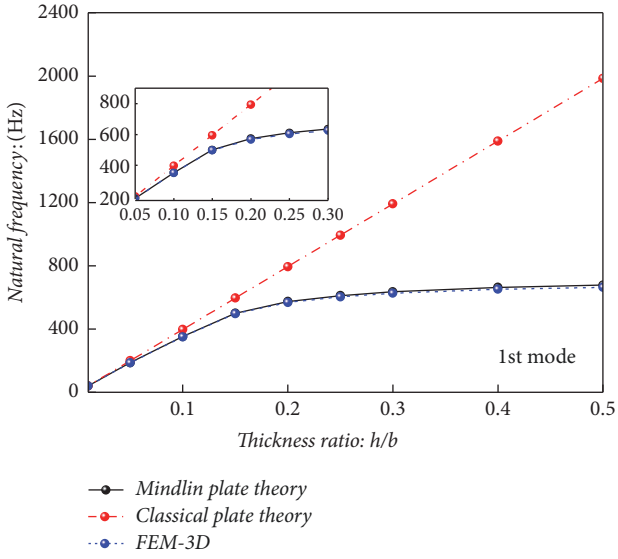

(a) The frequency of 4 clamped points' plate with different thickness ratios h/b and theories

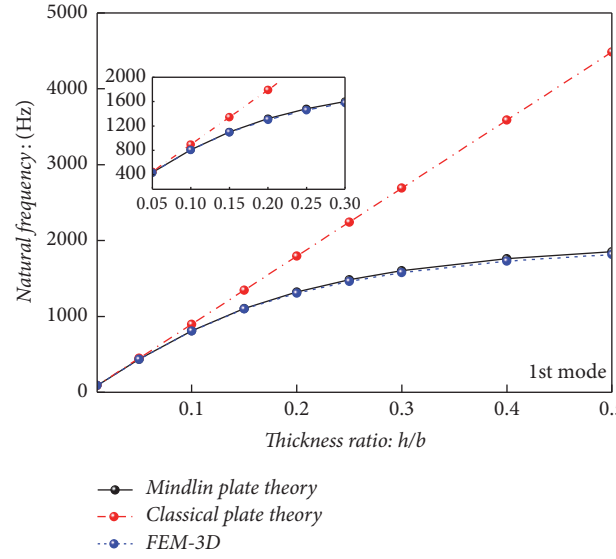

(b) The frequency of 16 clamped points' plate with different thickness ratios h/b and theories

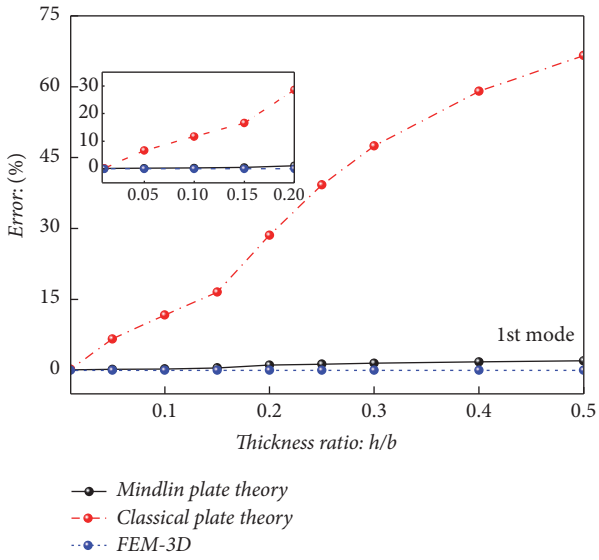

(c) Error (%) of 4 clamped points' plate with different thickness ratios h/b and theories

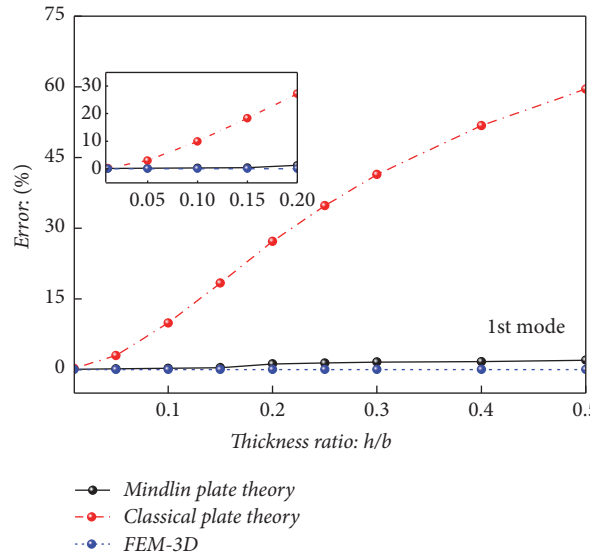

(d) Error (%) of 16 clamped points' plate with different thickness ratios h/b and theories

FIGURE 12: The frequency and error (%) of multipoint-supported plates with different thickness ratios h/b and theories.

$$\{Q_{1-2}\}_{n+1,t} = -\overline{\delta}_{bn}\delta_{nn'} \tag{B.11}$$

$$\{Q_{1-3}\}_{n+1,t} = 0 \tag{B.12}$$

$$\{C_{1-1}\}_{s,t} = -\left(\lambda_{am}^2 + \lambda_{bn}^2\right)\delta_{st} \tag{B.13}$$

$$\{C_{1-2}\}_{s,t} = \delta_{st}\sum_{p=0}^{\infty}\left(-\lambda_{ap}\right)\tau_{ap}^{m} \tag{B.14}$$

$$\{C_{1-3}\}_{s,t} = \delta_{st}\sum_{q=0}^{\infty}\left(-\lambda_{bq}\right)\kappa_{bq}^{n} \tag{B.15}$$

$$\{D_{1-1}\}_{s,m'+1} = \left(\varphi_{1n} + \beta_{1n}\left(-\lambda_{am}^2\right)\right)\delta_{mm'} \tag{B.16}$$

$$\{D_{1-2}\}_{s,m'+1} = \left(\varphi_{2n} + \beta_{2n}\left(-\lambda_{am}^2\right)\right)\delta_{mm'} \tag{B.17}$$

$$\{D_{1-3}\}_{s,n'+1} = \left(\phi_{1m} + \alpha_{1m}\left(-\lambda_{bn}^2\right)\right)\delta_{nn'} \tag{B.18}$$

$$\{D_{1-4}\}_{s,n'+1} = \left(\phi_{2m} + \alpha_{2m}\left(-\lambda_{bn}^2\right)\right)\delta_{nn'} \tag{B.19}$$

$$\{D_{1-5}\}_{s,m'+1} = \delta_{mm'}\sum_{p=0}^{\infty}\left(-\lambda_{ap}\right)\tau_{ap}^{m}\beta_{1n} \tag{B.20}$$

$$\{D_{1-6}\}_{s,m'+1} = \delta_{mm'}\sum_{p=0}^{\infty}\left(-\lambda_{ap}\right)\tau_{ap}^{m}\beta_{2n} \tag{B.21}$$

$$\{D_{1-7}\}_{s,n'+1} = \gamma_{1m}\delta_{nn'} \tag{B.22}$$

$$\{D_{1-8}\}_{s,n'+1} = \gamma_{2m}\delta_{nn'} \tag{B.23}$$

$$\{D_{1-9}\}_{s,m'+1} = \delta_{mm'}\eta_{1n} \tag{B.24}$$

$$\{D_{1-10}\}_{s,m'+1} = \delta_{mm'}\eta_{2n} \tag{B.25}$$

$$\{D_{1-11}\}_{s,n'+1} = \delta_{nn'}\alpha_{1m}\sum_{q=0}^{\infty}\left(-\lambda_{bq}\right)\kappa_{bq}^{n} \tag{B.26}$$

$$\{D_{1-12}\}_{s,n'+1} = \delta_{nn'}\alpha_{2m}\sum_{q=0}^{\infty}\left(-\lambda_{bq}\right)\kappa_{bq}^{n} \tag{B.27}$$

$$\begin{aligned}\{E_{1-1}\}_{s,t} &= \delta_{st},\\ \{E_{1-2}\}_{s,t} &= 0,\\ \{E_{1-3}\}_{s,t} &= 0\end{aligned} \tag{B.28}$$

$$\{F_{1-1}\}_{s,m'+1} = \beta_{1n}\delta_{mm'} \tag{B.29}$$

$$\{F_{1-2}\}_{s,m'+1} = \beta_{2n}\delta_{mm'} \tag{B.30}$$

$$\{F_{1-3}\}_{s,n'+1} = \alpha_{1m}\delta_{nn'} \tag{B.31}$$

$$\{F_{1-4}\}_{s,n'+1} = \alpha_{2m}\delta_{nn'} \tag{B.32}$$

$$\{F_{1-5}\}_{s,m'+1} = \{F_{1-6}\}_{s,m'+1} = 0 \tag{B.33}$$

$$\{F_{1-7}\}_{s,n'+1} = \{F_{1-8}\}_{s,n'+1} = 0 \tag{B.34}$$

$$\{F_{1-9}\}_{s,m'+1} = \{F_{1-10}\}_{s,m'+1} = 0 \tag{B.35}$$

$$\{F_{1-11}\}_{s,n'+1} = \{F_{1-12}\}_{s,n'+1} = 0 \tag{B.36}$$

Data Availability

The data used to support the findings of this study are available from the corresponding author upon request.

Conflicts of Interest

The authors declare that they have no conflicts of interest.

Acknowledgments

This study was funded by the National Key Research and Development Program (2016YFC0303406), Ph.D. Student Research and Innovation Fund of the Fundamental Research Funds for the Central Universities (HEUGIP201801), Fundamental Research Funds for the Central Universities (HEUCFM170113), High Technology Ship Funds of Ministry of Industry and Information of P.R. China, National Natural Science Foundation of China (nos. 51209052 and 51709063), Assembly Advanced Research Fund of China (no. 6140210020105), China Postdoctoral Science Foundation (no. 2014M552661), Major Innovation Projects of High Technology Ship Funds of Ministry of Industry and Information of P.R. China, and Naval Pre-Research Project.

References

[1] R. Mindlin, "Influence of rotatory inertia and shear on flexural motions of isotropic, elastic plates," *Journal of Applied Mechanics*, vol. 18, p. 31, 1951.

[2] C. S. Huang and K. H. Ho, "An analytical solution for vibrations of a polarly orthotropic Mindlin sectorial plate with simply supported radial edges," *Journal of Sound and Vibration*, vol. 273, no. 1-2, pp. 277–294, 2004.

[3] F. Ohya, M. Ueda, T. Uchiyama, and M. Kikuchi, "Free vibration analysis by the superposition method of rectangular Mindlin plates with internal columns resting on uniform elastic edge supports," *Journal of Sound and Vibration*, vol. 289, no. 1-2, pp. 1–24, 2006.

[4] Y. Xiang, S. K. Lai, L. Zhou, and C. W. Lim, "DSC-Ritz element method for vibration analysis of rectangular Mindlin plates with mixed edge supports," *European Journal of Mechanics - A/Solids*, vol. 29, no. 4, pp. 619–628, 2010.

[5] L. B. Rao and C. K. Rao, "Free vibration of circular plates with elastic edge support and resting on an elastic foundation," *International Journal of Acoustics and Vibration*, vol. 17, no. 4, pp. 204–207, 2012.

[6] M. Takashi and Y. Jin, "Application of the collocation method to vibration analysis of rectangular mindlin plates," *Computers & Structures*, vol. 18, no. 3, pp. 425–431, 1984.

[7] F. Jiarang and Y. Jianqiao, "An exact solution for the statics and dynamics of laminated thick plates with orthotropic layers," *International Journal of Solids and Structures*, vol. 26, no. 5-6, pp. 655–662, 1990.

[8] S. Hosseini-Hashemi, M. Fadaee, and S. R. Atashipour, "A new exact analytical approach for free vibration of Reissner–Mindlin functionally graded rectangular plates," *International Journal of Mechanical Sciences*, vol. 53, no. 1, pp. 11–22, 2011.

[9] L. Dozio and E. Carrera, "A variable kinematic Ritz formulation for vibration study of quadrilateral plates with arbitrary thickness," *Journal of Sound and Vibration*, vol. 330, no. 18-19, pp. 4611–4632, 2011.

[10] R. Maretic and V. Glavardanov, "Vibration of circular plate with an internal elastic ring support under exterior edge pressure," *International Journal of Structural Stability and Dynamics*, vol. 14, no. 1, Article ID 1350053, 2014.

[11] E. Bahmyari and M. R. Khedmati, "Vibration analysis of nonhomogeneous moderately thick plates with point supports resting on Pasternak elastic foundation using element free Galerkin method," *Engineering Analysis with Boundary Elements*, vol. 37, no. 10, pp. 1212–1238, 2013.

[12] S. Bashmal, R. Bhat, and S. Rakheja, "In-plane free vibration analysis of an annular disk with point elastic support," *Shock and Vibration*, vol. 18, no. 4, pp. 627–640, 2011.

[13] Ü. Esendemir, "An Elastic-plastic Stress Analysis in a Polymer-Matrix Composite Beam of Arbitrary Orientation Supported from Two Ends Acted Upon with A Force at the Mid Point," *Journal of Reinforced Plastics and Composites*, vol. 23, no. 6, pp. 613–623, 2004.

[14] M. A. Foyouzat and H. E. Estekanchia, "Dynamic response of thin plates on time-varying elastic point supports," *Structural Engineering and Mechanics*, vol. 62, no. 4, pp. 431–441, 2017.

[15] B. S. Gan, N. D. Kien, and L. T. Ha, "Effect of intermediate elastic support on vibration of functionally graded Euler-Bernoulli beams excited by a moving point load," *Journal of Asian Architecture and Building Engineering*, vol. 16, no. 2, pp. 363–369, 2017.

[16] M. Küçük, H. Akbulut, and Ü. Esendemir, "An elastic-plastic stress analysis of aluminum metal-matrix composite beams supported from two ends with a force acted at the mid point," *Journal of Reinforced Plastics and Composites*, vol. 21, no. 15, pp. 1363–1375, 2002.

[17] H. Bakhshi Khaniki and S. Hosseini-Hashemi, "Dynamic transverse vibration characteristics of nonuniform nonlocal strain gradient beams using the generalized differential quadrature method," *The European Physical Journal Plus*, vol. 132, no. 11, article no. 500, 2017.

[18] H. Bakhshi Khaniki and S. Hosseini-Hashemi, "Buckling analysis of tapered nanobeams using nonlocal strain gradient theory and a generalized differential quadrature method," *Materials Research Express*, vol. 4, no. 6, Article ID 065003, 2017.

[19] H. B. Khaniki, S. Hosseini-Hashemi, and A. Nezamabadi, "Buckling analysis of nonuniform nonlocal strain gradient beams using generalized differential quadrature method," *Alexandria Engineering Journal*, 2017.

[20] A. R. Setoodeh and G. Karami, "Static, free vibration and buckling analysis of anisotropic thick laminated composite plates on distributed and point elastic supports using a 3-D layer-wise FEM," *Engineering Structures*, vol. 26, no. 2, pp. 211–220, 2004.

[21] Y. Xu and D. Zhou, "Three-dimensional elasticity solution of simple-supported rectangular plate on point supports, line supports and elastic foundation," *Science China Technological Sciences*, vol. 52, no. 3, pp. 584–589, 2009.

[22] L. H. Wu, "Free vibrations of arbitrary quadrilateral thick plates with internal columns and uniform elastic edge supports by pb-2 Ritz method," *Structural Engineering and Mechanics*, vol. 44, no. 3, pp. 267–288, 2012.

[23] L. H. Wu and Y. Lu, "Free vibration analysis of rectangular plates with internal columns and uniform elastic edge supports by pb-2 Ritz method," *International Journal of Mechanical Sciences*, vol. 53, no. 7, pp. 494–504, 2011.

[24] S. Hosseini Hashemi and H. Bakhshi Khaniki, "Vibration analysis of a timoshenko non-uniform nanobeam based on nonlocal theory: An analytical solution," in *Proceedings of the International Journal of Nano Dimension*, vol. 8, pp. 70–81, 2017.

[25] H. B. Khaniki, "On vibrations of nanobeam systems," *International Journal of Engineering Science*, vol. 124, pp. 85–103, 2018.

[26] H. B. Khaniki, "Vibration analysis of rotating nanobeam systems using Eringen's two-phase local/nonlocal model," *Physica E: Low-dimensional Systems and Nanostructures*, 2018.

[27] S. Rajasekaran and H. Bakhshi Khaniki, "Finite element static and dynamic analysis of axially functionally graded nonuniform small-scale beams based on nonlocal strain gradient theory," *Mechanics of Advanced Materials and Structures*, pp. 1–15, 2018.

[28] S. Rajasekaran and H. B. Khaniki, "Bending, buckling and vibration of small-scale tapered beams," *International Journal of Engineering Science*, vol. 120, pp. 172–188, 2017.

[29] Q. Wang, D. Shao, and B. Qin, "A simple first-order shear deformation shell theory for vibration analysis of composite laminated open cylindrical shells with general boundary conditions," *Composite Structures*, vol. 184, pp. 211–232, 2018.

[30] Y. Zhou, Q. Wang, D. Shi, Q. Liang, and Z. Zhang, "Exact solutions for the free in-plane vibrations of rectangular plates with arbitrary boundary conditions," *International Journal of Mechanical Sciences*, vol. 130, pp. 1–10, 2017.

[31] Q. Wang, B. Qin, D. Shi, and Q. Liang, "A semi-analytical method for vibration analysis of functionally graded carbon nanotube reinforced composite doubly-curved panels and shells of revolution," *Composite Structures*, vol. 174, pp. 87–109, 2017.

[32] Q. Wang, X. Cui, B. Qin, Q. Liang, and J. Tang, "A semi-analytical method for vibration analysis of functionally graded (FG) sandwich doubly-curved panels and shells of revolution," *International Journal of Mechanical Sciences*, vol. 134, pp. 479–499, 2017.

[33] F. Pang et al., "A semi analytical method for the free vibration of doubly-curved shells of revolution," *Computers & Mathematics with Applications*, vol. 75, no. 9, pp. 3249–3268, 2018.

[34] F. Pang, H. Li, K. Choe, D. Shi, and K. Kim, "Free and Forced Vibration Analysis of Airtight Cylindrical Vessels with Doubly Curved Shells of Revolution by Using Jacobi-Ritz Method," *Shock and Vibration*, vol. 2017, Article ID 4538540, 20 pages, 2017.

[35] X. Guan, J. Tang, Q. Wang, and C. shuai, "Application of the differential quadrature finite element method to free vibration of elastically restrained plate with irregular geometries," *Engineering Analysis with Boundary Elements*, vol. 90, pp. 1–16, 2018.

[36] X. Guan, J. Tang, D. Shi, C. shuai, and Q. Wang, "A semi-analytical method for transverse vibration of sector-like thin plate with simply supported radial edges," *Applied Mathematical Modelling: Simulation and Computation for Engineering and Environmental Systems*, vol. 60, pp. 48–63, 2018.

[37] Q. Wang, X. Cui, B. Qin, and Q. Liang, "Vibration analysis of the functionally graded carbon nanotube reinforced composite shallow shells with arbitrary boundary conditions," *Composite Structures*, vol. 182, pp. 364–379, 2017.

[38] L. Li, H. Li, F. Pang, X. Wang, Y. Du, and S. Li, "The modified Fourier-Ritz approach for the free vibration of functionally graded cylindrical, conical, spherical panels and shells of revolution with general boundary condition," *Mathematical Problems in Engineering*, Art. ID 9183924, 32 pages, 2017.

[39] H. Li, F. Pang, X. Wang, and S. Li, "Benchmark Solution for Free Vibration of Moderately Thick Functionally Graded Sandwich Sector Plates on Two-Parameter Elastic Foundation with General Boundary Conditions," *Shock and Vibration*, vol. 2017, Article ID 4018629, 35 pages, 2017.

[40] F. Pang, H. Li, Y. Du, Y. Shan, and F. Ji, "Free Vibration Of Functionally Graded Carbon Nanotube Reinforced Composite Annular Sector Plate With General Boundary Supports," *Curved and Layered Structures*, vol. 5, no. 1, pp. 49–67, 2018.

[41] J. Guo, D. Shi, Q. Wang, J. Tang, and C. Shuai, "Dynamic analysis of laminated doubly-curved shells with general boundary conditions by means of a domain decomposition method," *International Journal of Mechanical Sciences*, vol. 138-139, pp. 159–186, 2018.

[42] F. Pang, H. Li, X. Miao, and X. Wang, "A modified Fourier solution for vibration analysis of moderately thick laminated annular sector plates with general boundary conditions, internal radial line and circumferential arc supports," *Curved and Layered Structures*, vol. 4, no. 1, pp. 189–220, 2017.

[43] H. Li, F. Pang, X. Miao, Y. Du, and H. Tian, "A semi-analytical method for vibration analysis of stepped doubly-curved shells of revolution with arbitrary boundary conditions," *Thin-Walled Structures*, vol. 129, pp. 125–144, 2018.